1-1-2012

Cassini UVIS observations of Titan nightglow spectra

Joseph M. Ajello

Robert A. West

Jacques Gustin

Kristopher Larsen

A. Ian F. Stewart

See next page for additional authors

Recommended Citation

Authors

Joseph M. Ajello, Robert A. West, Jacques Gustin, Kristopher Larsen, A. Ian F. Stewart, Larry W. Esposito, William E. McClintock, Gregory M. Holsclaw, and E. Todd Bradley

Cassini UVIS observations of Titan nightglow spectra

Joseph M. Ajello,[1] Robert A. West,[1] Jacques Gustin,[2] Kristopher Larsen,[3] A. Ian F. Stewart,[3] Larry W. Esposito,[3] William E. McClintock,[3] Gregory M. Holsclaw,[3] and E. Todd Bradley[4]

[1]   In this paper we present the first nightside EUV and FUV airglow limb spectra of Titan showing molecular emissions. The Cassini Ultraviolet Imaging Spectrograph (UVIS) observed photon emissions of Titan's day and night limb-airglow and disk-airglow on multiple occasions, including during an eclipse observation. The 71 airglow observations analyzed in this paper show EUV (600–1150 Å) and FUV (1150–1900 Å) atomic multiplet lines and band emissions arising from either photoelectron induced fluorescence and solar photo-fragmentation of molecular nitrogen (N_2) or excitation by magnetosphere plasma. The altitude of the peak UV emissions on the limb during daylight occurred inside the thermosphere at the altitude of the topside ionosphere (near 1000 km altitude). However, at night on the limb, a subset of emission features, much weaker in intensity, arise in the atmosphere with two different geometries. First, there is a twilight photoelectron-excited glow that persists with solar depression angle up to 25–30 degrees past the terminator, until the solar XUV shadow height passes the altitude of the topside ionosphere (1000–1200 km). The UV twilight glow spectrum is similar to the dayglow but weaker in intensity. Second, beyond 120° solar zenith angle, when the upper atmosphere of Titan is in total XUV darkness, there is indication of weak and sporadic nightside UV airglow emissions excited by magnetosphere plasma collisions with ambient thermosphere gas, with similar N_2 excited features as above in the daylight or twilight glow over an extended altitude range.

Citation: Ajello, J. M., R. A. West, J. Gustin, K. Larsen, A. I. F. Stewart, L. W. Esposito, W. E. McClintock, G. M. Holsclaw, and E. T. Bradley (2012), Cassini UVIS observations of Titan nightglow spectra, *J. Geophys. Res.*, *117*, A12315, doi:10.1029/2012JA017888.

1.   Introduction

[2]   There are four nitrogen-bearing atmospheres in the solar system: Titan, Triton, Earth and Pluto. The complex UV airglow signatures of N_2 and its dissociation products from the mesosphere and thermosphere are the principal means of studying the energy input to a planetary atmosphere. The response of the Titan upper atmosphere to both the solar cycle variation of the solar extreme ultraviolet (XUV) and local magnetosphere particle injection is a prime focus of the Cassini Mission. Based on Cassini in situ data, *Strobel*

and Cui [2012] have shown that the globally averaged magnetosphere energy input to Titan's upper atmosphere is almost always smaller than the solar XUV.

[3]   Photoelectron excitation dominates the Titan dayside airglow spectrum [*Stevens et al.*, 2011]. Energetic protons (H^+) and O^+ ions have been observed by Cassini/Magnetosphere Imaging Instrument (MIMI) and thermal and suprathermal ions are studied by Cassini Plasma Spectrometer (CAPS) in Saturn's outer magnetosphere. These particles can precipitate into Titan's atmosphere where they deposit energy, generating airglow emissions and driving ionospheric chemistry for both the lower atmosphere ionosphere and topside ionosphere [*Sittler et al.*, 2010a, 2010b; *Cravens et al.*, 2008; *Ledvina et al.*, 2005; *Lavvas et al.*, 2011; *Westlake et al.*, 2011; *Fulchignoni et al.*, 2005; *Gan et al.*, 1992; *Smith et al.*, 2009; *Shah et al.*, 2009]. The energies of the upstream magnetosphere plasma ions interacting with Titan's thermosphere (400–1400 km) extend over a large energy range from 0.1 keV to 4 MeV for protons, from 2 keV to 4 MeV for oxygen ions [*Cravens et al.* 2008] and 10 eV to 10 keV for electrons [*Cravens et al.*, 2008, 2009]. Either energetic electron or proton interactions with ambient neutral species can be a significant source of nightglow emissions [*Ajello et al.*, 2010, 2011a, 2011b].

[1]Jet Propulsion Laboratory, California Institute of Technology, Pasadena, California, USA.

[2]Laboratoire de Physique Atmosphérique et Planétaire, Université de Liège, Liège, Belgium.

[3]Laboratory for Atmospheric and Space Physics, University of Colorado Boulder, Boulder, Colorado, USA.

[4]Department of Physics, University of Central Florida, Orlando, Florida, USA.

Corresponding author: J. M. Ajello, Jet Propulsion Laboratory, California Institute of Technology, Pasadena, CA 91109, USA. (joseph.m.ajello@jpl.nasa.gov)

[4] Titan is lacking significant intrinsic magnetization, and is normally immersed in Saturn's rapidly rotating magnetosphere allowing direct access of the co-rotating plasma to the thermosphere region [*Westlake et al.*, 2011; *De La Haye et al.*, 2007]. Saturn's magnetospheric interaction with Titan from recent results of CAPS and Cassini magnetometer (MAG) show the upstream flow appears composed of intense light ions (protons (H^+) and H_2^+) and the heavier ion O^+ [*Sittler et al.*, 2010b]. The altitude deposition ranges of protons and O^+ (the second most abundant ion in the co-rotating plasma) indicates an extended nighttime ionosphere layer excitation source below 1000 km [*Cravens et al.*, 2008] and verified recently by *Kliore et al.* [2008] by the radio occultation experiment discovery of the lower sporadic ionosphere. According to *Kliore et al.* [2008], there is a ionospheric peak for one of the polar observations in the region of 500–600 km. The energy deposition rates of the upper atmosphere from 600 to 1500 km by precipitating ions, H^+ and O^+ have been modeled by *Westlake et al.* [2011] using Cassini Ion and Neutral Mass Spectrometer (INMS) data. The observations show that Titan's N_2 global thermosphere distribution quickly responds to both O^+ energy deposition that peaks at 1100 km and H^+ energy deposition that peaks at 700 km.

[5] To date we have published UV results from two Cassini Titan passes. Analyses of the 13 December 2004 (13Dec04, TB) and 22 June 2009 (22 June 09, T57) Titan dayside observations of the extreme ultraviolet (EUV: 900–1140 Å) and the far ultraviolet (FUV: 1150–1900 Å) disk and limb spectra from the Ultraviolet Imaging Spectrometer (UVIS) on Cassini have been recently published. These two observation dates were chosen for analysis because of particularly high S/N in their dayglow spectra. We refer to the UVIS publications of these two observations as Paper 1 [*Ajello et al.*, 2007], Paper 2 [*Ajello et al.*, 2008], and Paper 3 [*Stevens et al.*, 2011], respectively. Model spectral fits to the Titan FUV disk dayglow disk spectrum of 13Dec04 described in Paper 2 and to the Titan FUV limb spectrum of 22June09 in Paper 3 revealed that Titan's FUV dayglow emission is attributed to five main sources: (1) the Lyman-Birge-Hopfield (LBH) band system of N_2 (a $^1\Pi_g - X\ ^1\Sigma_g^+$) due to photoelectrons produced by solar XUV on N_2 [*Young et al.*, 2010; *Ajello and Shemansky*, 1985; *Ajello et al.*, 2010]; (2) N I multiplets primarily due to solar photodissociative ionization (PDI) excitation of N_2 [*Meier et al.*, 1991; *Samson et al.*, 1991; *Mumma and Zipf*, 1971]; (3) the H Lyα emission line excited mainly by solar fluorescence at 1215.6 Å; (4) the N_2 Vegard-Kaplan (VK) band system ($A^3\Sigma_u^+ \rightarrow X^1\Sigma_g^+$) peaking near 900 km altitude also from photoelectrons [*Stevens et al.*, 2011; *Shemansky*, 1969]; and (5) reflected sunlight, predominantly arising from altitudes below 800 km and wavelengths longward of 1500 Å. The first four sources are the same as observed in the thermosphere of the Earth by the Far Ultraviolet Spectrographic Explorer (FUSE) instrument and other earth-orbiting spacecraft [*Bishop and Feldman*, 2003; *Bishop et al.*, 2007; *Broadfoot et al.*, 1997; *Feldman et al.*, 2001; *Morrison et al.*, 1990].

[6] The electronic excitations proceeding from the $X\ ^1\Sigma_g^+$ ground-state to several closely spaced (~12–15 eV) states are the source of molecular emissions in the EUV observed by spacecraft, and have been discussed in Paper 1 for 13Dec04 and Paper 3 for 22June09. Two of the excited states, b $^1\Pi_u$, b' 1Σ are nominally valence in character and three others; $c_3{}^1\Pi_u$, $o_3\ ^1\Pi_u$, and $c_4'\ ^1\Sigma_u^+$ are Rydberg states with principal quantum number n = 3. Because of the presence of strong homogeneous and heterogeneous interactions they are referred to here as Rydberg-valence (RV) states. The spectrum is weakly to-strongly predissociated by an indirect mechanism involving multiple states of $^3\Pi_u$ and $^1\Sigma^+$ symmetry, some of which are unbound. Because of this, the predissociation to emission branching ratio varies haphazardly from almost zero to unity, leading to significant emission and predissociation cross sections that are the main source of the observed EUV N_2 and atomic N emissions by the UVIS [*Lewis et al.*, 2005a, 2005b, 2008a, 2008b; *Ubachs et al.*, 2001; *Liu et al.*, 2005; *Shemansky et al.*, 1995; *Ajello et al.*, 1989; J. M. Ajello, A. N. Heays, B. R. Lewis and S. Gibson, High-resolution EUV spectrum of N_2 by electron impact, submitted to *The Astrophysical Journal Supplement*, 2012].

[7] No levels of the $c_3{}^1\Pi_u$ and $o_3\ ^1\Pi_u$ states are expected to appear here in emission because they are very efficiently predissociated. The presence of emission from the b' $^1\Sigma_u^+$ state, is inferred from the orbit TB analysis of *Ajello et al.* [2007] as there are no sharp and strong features from this transition [*Ajello et al.*, 1989; submitted manuscript]. Further members of the $c_3\ ^1\Pi_u$ and $c_4'\ ^1\Sigma_u^+$ Rydberg series with n > 3 were found to emit in the EUV, with high-resolution observations made by *Roncin et al.* [1998] and emission cross sections reported in *Ajello et al.* [2010; submitted manuscript].

[8] In this paper we analyze 71 limb observations from 19 April, 2009 to 28 January, 2010 of Titan to search for darkside UV emissions and trace the variability in dayglow, twilight glow and nightglow emission intensities from the parent molecule N_2, the major species of the upper atmosphere of Titan [*De La Haye et al.*, 2007]. Some of the important geometric variables for strong locally occurring (latitude and altitude) UV dayglow are solar zenith angle (SZA) and associated target center phase angle (TPA), Solar XUV, and minimum ray height (MRH) at the limb. Nightglow emissions, which can be generated throughout the thermosphere arising from interactions with the co-rotating magnetosphere from 400 to 1400 km, indicate that the solar-incidence-RAM angle (SRA or RAM) and Titan latitude are important for determining the side and latitude of Titan illuminated by the plasma stream. Using published literature *Sittler et al.* [2010a] estimated that particle energy input can rival the solar XUV; this estimate was recently proven erroneous by *Strobel and Cui* [2012]. These 71 observations in 2009–2010 took place at time of solar minimum as compared to Paper 1 observation of orbit Tb that occurred at time in 2004 that the UV solar flux was still weak in solar cycle 24, though not at solar minimum. We also analyze one Titan observation from 25 March 2008 near solar minimum that presented strong daylight and twilight glow emissions from both the limb and the disk. *Rymer et al.* [2009] point out that that low solar activity allows fewer magnetosheath plasma interactions with Titan. Low solar activity allows a larger magnetosphere as the solar wind pressure weakens compared to solar maximum. Most encounters in our time frame occur as the plasma sheet category [see *Rymer et al.*, 2009].

[9] Many of these 71 observations contain daylight disk and nightside disk observations as well as the limb. The geometry for a limb observation is shown in Figure 1 to
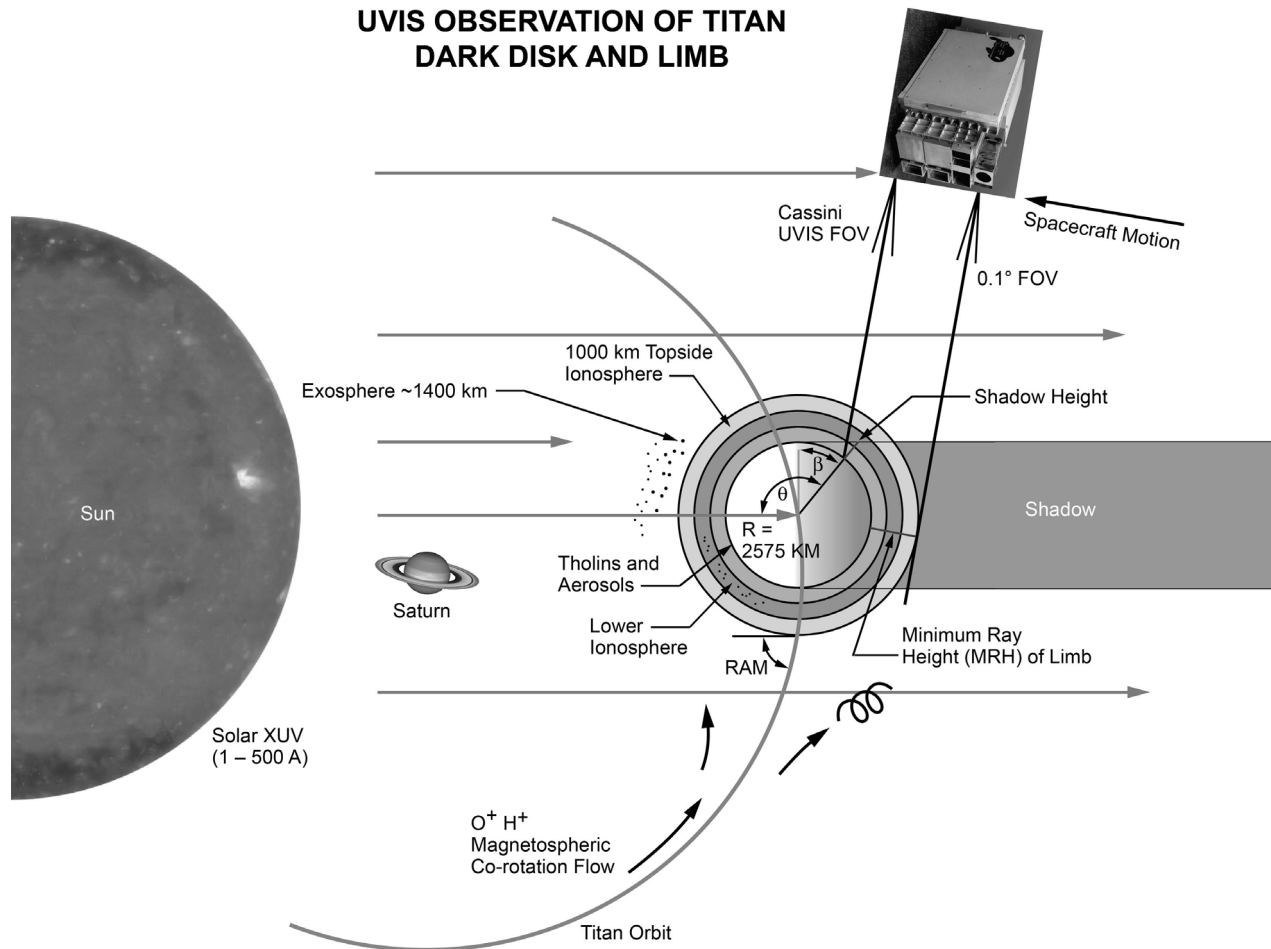
UVIS OBSERVATION OF TITAN
DARK DISK AND LIMB

Figure 1. Nighttime viewing geometry of the UVIS limb and disk observations at a solar depression angle of β through an atmosphere composed of a major gas, N_2 (96%), and four distinct optical/UV layers: 1) haze (complex organic solids), surface to 400 km; 2) lower thermosphere (400–800 km), including the lower ionosphere and a UV optically thick (10–1400 Å) distribution of CH_4 [*Kliore et al.*, 2008]; 3) upper thermosphere (800–1400 km), including the topside ionosphere [*Stevens et al.*, 2011]; and 4) the exosphere (above 1400 km). The UVIS FUV (EUV) FOV for the low-resolution slit is 1.5 mrad × 60 mrad (2.0 mrad × 60 mrad) and is shown as 0.1°FOV in the diagram. The figure shows the four main layers of Titan's atmosphere illuminated by the Sun and interacting with the upstream magnetosphere flow of abundant ions: H^+ and O^+ at a RAM angle of 90°. The drawing indicates the presence of a shadow height an important altitude for twilight and nighttime observations. The shadow height is a function of solar depression angle. The MRH of a limb observation is also indicated.

remind us of the four atmosphere layers: 1) a distribution of haze (complex solid organics) or aerosols in the lower atmosphere (mesosphere) that persist up to an altitude of 400–500 km (or higher for detached haze layers [*Tomasko and West*, 2010], as we have shown in a set of altitude-dependent FUV spectra demonstrating strong UV particulate, Rayleigh and Mie scattering, and reflection above 1500 Å in *Sittler et al.* [2010a, Figure 16.24]; 2) the lower thermosphere, where the temperature is about ~170 K at 400 km and decreases with altitude (400–800 km) and the sporadic middle ionosphere appears [*Kliore et al.*, 2008]; 3) the topside ionosphere from 800 to 1400 km, which is the source region of the UV dayglow; and 4) the exosphere above ~1400 km. The haze or aerosol layer (and CH_4 slant optical depth of unity in the XUV) may act as a secondary (tertiary) planetary absorbing surface for solar FUV (and XUV)

radiation and for many years made Titan appear to be the largest moon in the solar system until Voyager observations.

[10]   The shadow heights for the solar XUV and the solar FUV are important quantities for an extended atmosphere like Titan. For example, the ionosphere (airglow layer peak intensity at 1000 km altitude) represents 40% of the radius of the satellite (2576 km) compared to Earth with a 3% value for the ratio of the E, F ionosphere region/airglow layer to the radius (6378 km). From Figure 1 we find that the shadow height z_{ion} for three optical wavelength ranges measured from the satellite surface as a function of solar depression angle, (β_{opt}) is given by

$$\cos\left(\beta_{opt}\right) = \left(R + h_{opt}\right)/\left(R + z_{ion}\right), \qquad (1)$$

where the subscript "opt" refers to a Titan radius (R + h_{opt}) altitude at the terminator where slant optical depth unity at the terminator occurs for near IR-visible wavelengths at minimum ray height altitude h_{opt} = 0 km, FUV (wavelengths above 1400 Å) at altitude h_{opt} = 300 km, and FUV, EUV XUV (wavelengths below 1400 Å) at altitude h_{opt} = 800 km, respectively. The three optical shadow heights occur for hard surface conditions, particulate haze or high energy photons (wavelengths below 1400 Å) by an absorbing methane distribution (for solar rays, see also *Ajello et al.* [1973, Figure 1]). The upper altitude of the topside ionosphere is at about z_{ion} = 1200 km and allows us to determine for the three optical ranges where the ionosphere/airglow layer is in solar darkness (Paper 1). We find the three solar depression angles are approximately 47°, 40° and 26°, respectively. A UVIS limb airglow observation for a SZA line of sight above 116° ensures darkness in the thermosphere and precludes till dawn diurnal enhancement of an ionosphere from solar XUV creation of photoelectrons. On the other hand, magnetosphere protons with energies above 30 keV can deeply penetrate the atmosphere and excite the FUV from N_2 (wavelengths above 1400 Å) for UV transmission at altitudes throughout the ionosphere, down to 500 km [*Cravens et al.*, 2008; see also *Sittler et al.*, 2010a, Figure 16.3].

2. The Airglow Observations

[11] The UVIS instrument includes a two-channel imaging spectrograph in the far ultraviolet (FUV: 1115–1912 Å) and extreme-ultraviolet (EUV: 563–1182 Å) [*Esposito et al.*, 2004]. The detector format for each channel is 1024 spectral pixels × 64 spatial pixels, with 4 of the spatial pixels needed for engineering read-out information of the UVIS FUV (or EUV). The UVIS measurements will record spectral data for 60 pixels numbered 3–62 and referred to as 0–59 in this paper. The Titan observations discussed here were taken with a spectral resolution of 5.0 Å (low-resolution mode) and a rectangular field of view of 1.5 (2.0) × 60 mrad for each pixel along the full FUV (EUV) slit.

[12] The calibration and instrument features of the UVIS are described in *Esposito et al.* [2004] and most recently by *Stevens et al.* [2011]. The primary standards used for determining the UVIS absolute radiometric sensitivity prior to launch were photodiodes made available by the National Institute for Standards and Technology (NIST). These standards were used to calibrate the UVIS. Measurements of the star Alpha Virginis (Spica) obtained during cruise (16–17 January 1999) agreed with previous stellar spectra to within 10% for both EUV and FUV channels, confirming the UVIS laboratory results. Periodic stellar calibrations (every 100 days on average since 2006) obtained during cruise and in orbit track changes in UVIS sensitivity. From these stellar observations we assess the UVIS calibration uncertainty to be 15% or better for all wavelengths.

[13] From 19 April 2009 through 28 January 2010, the UVIS instrument obtained 71 EUV/FUV spectral data pairs of Titan observations. Many of the observations occurred on the same Titan passes, numbered T53 through T66. The observation interruptions occurred because of sequenced pointing changes on Titan. During this period, the full 1024 wavelength channels × 60 spatial channels were employed for these observations without any spectral or spatial binning or windowing that would limit the information content of the

observations. These data files, including geometry are labeled by observation number in this work, with the first EUV/FUV pair on 19 April, 2009 through the last observation on 28 January 2010. We call these records of data and geometry "data cubes." We abbreviate these observations without parenthesis as F0, F1, etc., through F71. Each observation of the 2009/2010 set lasts at least 12 min with files F1 and F2, the smallest set consisting of 3 records of 4 min each and the largest including 31 records F67 with a maximum Titan observation time of 124 min per UV spectral channel. The UVIS instrument is angularly scanning between multiples of 4-min stops, nominally, at an angular slew rate to move the UVIS bore sight from the exobase observations of Titan on one side of the body to the other side (total distance in plane of sky of 6000–8000 km). The only exception occurred for F14 described by *Stevens et al.* [2011] which is a high S/N "stare" observation. The spacecraft motion is compensated by an equal and opposite spacecraft slew. Similarly the 7 May 2009 eclipse observation was a 2-hr "stare" at a Titan disk and limb within Saturn's shadow. In summary, the nominal angular slews across Titan occur in segments of multiples of four minutes so the start-stop times coincide with multiples of 4-min dwells for ISS imaging.

[14] We show an over plot of the relevant major geometry information (mean (averaged over records and pixels)] SZA (top) and mean tangent ray height distance – MRH (bottom)) in Figure 2 with the same color coding for each point to be used in identifying the chronological order of the 71 observational UVIS data cubes. The data-cubes are a three dimensional UVIS data file for each observation: spatial pixel, spectral pixel, and record number, the latter represents time. The color coding used in Figure 2 is black for F0, the first observation and red for F70, the last observation, with each record four minutes in length in pixel integration time. Fortunately the limb airglow observations analyzed here occurred successively in seven distinct time-ordered geometrical groups during 2009, labeled: A (T53), B (T54), C (T55), D (T56), E (T62), F (T62), G (T62, T63) in Figure 2. We identify in Figure 2 (top) the SZA range for the three types of limb observations: bright limb (0–90°), twilight limb (90–120°) and dark limb (120–180°). There is also a critical MRH window exhibited in Figure 2 (bottom) from 500 to 1400 km for observing the limb airglow. This is the altitude range for UV airglow generation for the entire breadth of the ionosphere: both solar photoelectron excited and magnetosphere plasma impacted. The Titan atmosphere has an optical depth of much greater than unity for the entire UVIS FUV and EUV spectral range for MRH altitudes below 350 km, implying the UVIS cannot observe the surface of Titan.

[15] We display an overview plot of the average airglow limb spectrum, averaged over all records, altitudes and SZA of each of the seven types of EUV and FUV limb spectra identified from the observational group of 71 from 2009 in Figures 3a and 3b. We also include an eighth limb observation displaying the 22 June 2009 "stare" observation (labeled F14), the brightest daylight airglow to date (discussed in Paper 3). Many of these 71 limb observations also involved disk observations that we do not consider in detail. The 15% uncertainty in absolute sensitivity calibration plus statistical S/N uncertainty leads to approximately a 30% root-sum-square uncertainty in the spectral intensities [*Stevens et al.*, 2011]. We will consider, in detail, one distinct airglow
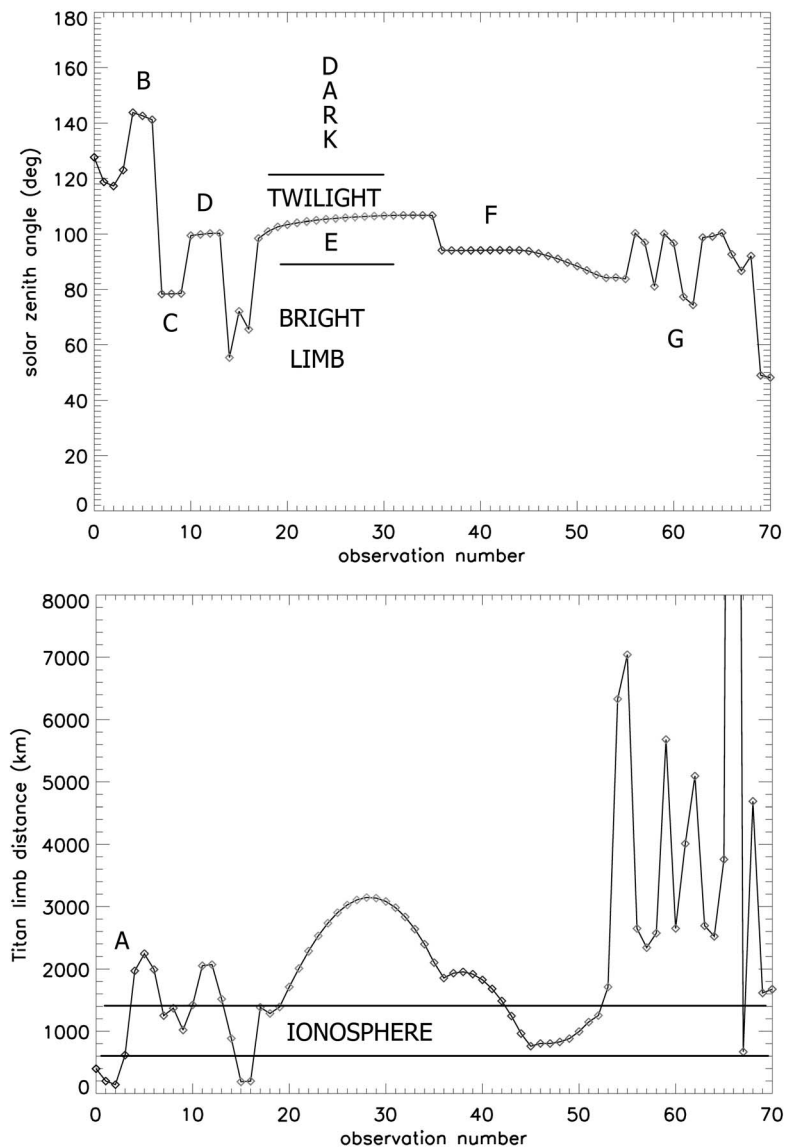
Figure 2. Over-plot of the major geometric parameters for the Titan limb observations with color coding from 0 (black) to 70 (red) according to observation number. These parameters are: (top) the mean SZA of the weighted mean pixel SZA for all the records of the observation; and (bottom) the mean Titan limb distance or MRH over all records of the observation. Figure 2 (top) shows the SZA regions for observing bright limb, twilight limb and dark limb observations. The seven different type of observations (labeled A,B,C,D,E,F, and G) with different geometric descriptions are identified in Table 1 by Titan flyby encounter number (column 1) and described (column 9).

observation from each of the seven groups, as identified by observation number in Figures 3a and 3b and Table 1. In addition, we consider the eclipse observation from 7May09 [*West et al.*, 2011, 2012] and the comprehensive set of 25March08 observations of the two limb crossings (bright and twilight) and the two disk observations (bright and twilight).

[16] We show the UVIS slit field-of-view (FOV) upon or near Titan at the middle of record 0 for each of the eight limb (and disk) observations in Figure 4. The geometric parameters from Figure 4 are listed in Table 1 and include the Titan flyby number, spacecraft distance to Titan center, the average MRH over the range of limb distances included in

the limb spectrum of the observation. The Table also includes the TPA and the mean SZA for the limb observation. The last column describes the limb observation description of Titan shown in Figures 3a and 3b for each of the observation types. For example, F48 that is initiated on 2009 DOY285 $15^h 05'$ is very bright in both the EUV and FUV with the slit spatial pixels on either the bright limb or bright disk at near $10°$ phase angle. F14 was the brightest afternoon limb observation and the slit center was maintained in position on the airglow layer near 800 km for the central spatial pixels MRH altitude for one hour. The brightest pixels were centered at 1000 km altitude. Most of the observations to be discussed
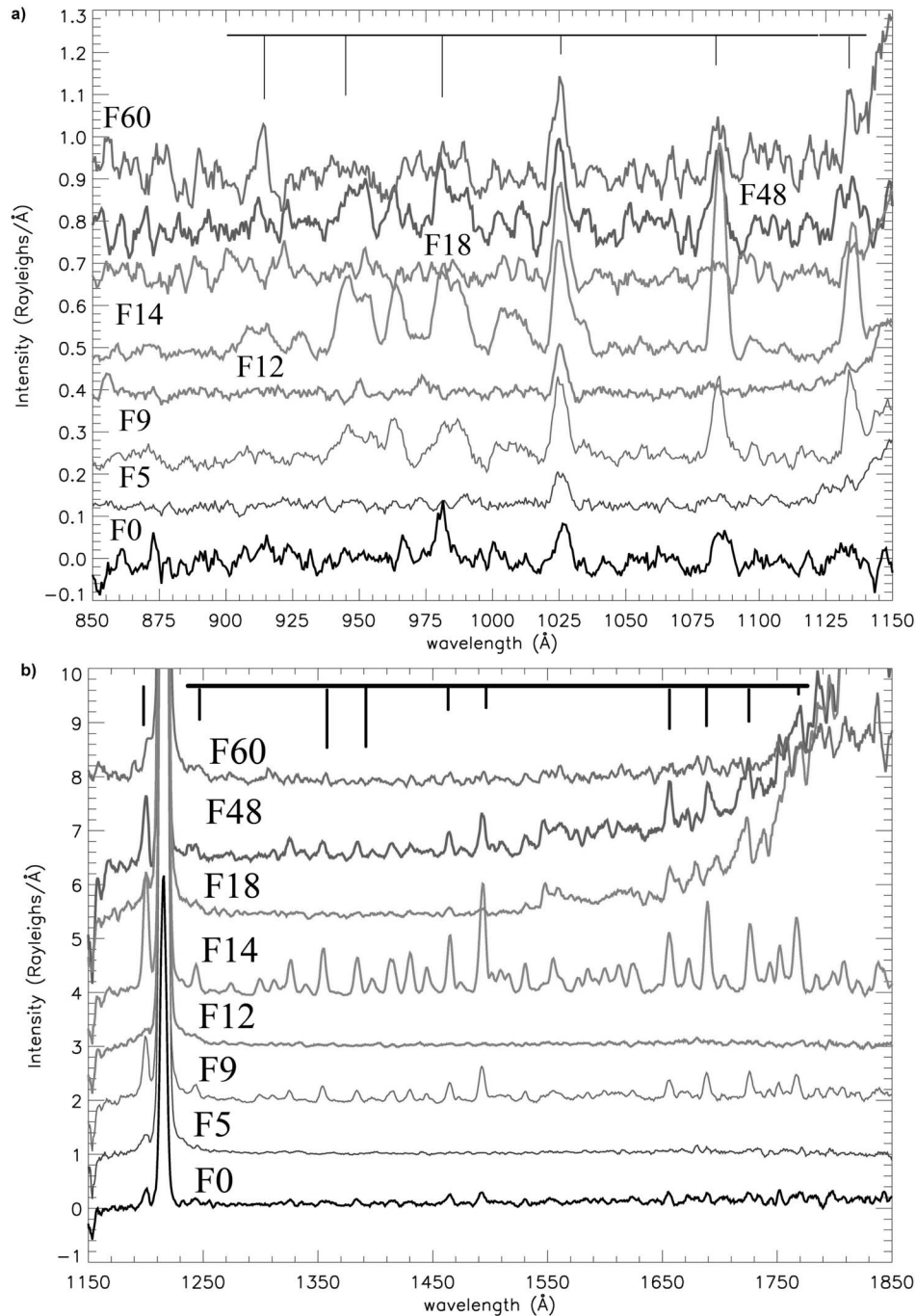
Figure 3. (a) EUV plots of individual limb spectra from regions A, B, C, D, E, F, and G of Figure 2 and described in first and last columns of Table 1. The observation number is given above each of the individual spectra. The color in the spectral plot corresponds to the same color as the corresponding observation number in Figure 2. The wavelength position of strong spectral emissions are indicated at the top of the plot. For example, the positions of NII (919 Å), N_2 c_4' $^1\Sigma_u^+$ ($v' = 4,3$) → X($v'' = 3,2$) at 945 Å, N I (953 Å), c_4' $^1\Sigma_u^+$ ($v' = 0$) → X($v'' = 1$) at 980 Å, H Lyβ at 1025 Å, N II (1085 Å), N I 1134 Å are indicated and are found to be especially strong on F14, 22 June 2009. (b) FUV plots of individual limb spectra from regions A, B, C, D, E, F, and G of Figure 3a and identified by Titan Flyby encounter number in column 1 of Table 1. (b) The observation number is given above each of the individual spectra. The color of the spectral plot corresponds to the same color as the corresponding observation number in Figure 2. The wavelength positions of strong spectral emissions are indicated at the top of the plot. For example, the wavelength positions of the strong vibrational bands of the Lyman-Birge-Hopfield band system (a $^1\Pi_g$ ($v' = 3, 2, 1$) → X $^1\Sigma_g^+$($v'' = 0, 1, 2$) of N_2, NI (1200, 1243, 1493) multiplets from solar photodissociative excitation of N_2 and several vibrational bands from the N_2 VK system ($A^3\Sigma_u^+$–$X^1\Sigma_g^+$ system) longward of 1550 Å are indicated.

Table 1. Geometry for Eight Types of Cassini UVIS EUV and FUV Observations in 2009

File (Titan Orbit)	File Name	Date	Number of 4-Min Records	S/C Distance to Titan (10³ km)	Mean Minimum Ray Height Limb Distance (Range-km)	Target Phase Angle (TPA)	Average Pixel Limb SZA (Range-Deg)	Limb Description
0 (T53)	EUV2009_109_23_06_00_UVIS_109 TI_FIRLMBAER001_CIRS	19 Apr	4	23.9	397 (200–800)	123	128 (115–130 deg)	DARK LOWER-LIMB
5 (T54)	EUV2009_126_02_11_10_UVIS_110 TI_EUVFUV001_PRIME	6 May	13	63.3	2254 (2100–2600)	65	143 (130–150)	DARK UPPER-LIMB
9 (T55)	EUV2009_141_18_16_27_UVIS_111 TI_EUVFUV001_PRIME	21 May	10	62.0	1020 (1000–1600)	123	78 (60–100)	AFTERNOON LIMB
12 (T56)	EUV2009_157_23_40_37_UVIS_112 TI_EUVFUV001_PRIME	6 Jun	13	71.3	2072 (1800–2400)	46	100 (80–115)	TWILIGHT LIMB
14 (T57)	EUV2009_173_22_15_16_39_000_U VIS_113TI_EUVFUV003_PRIME	22 Jun	15	63.9	884 (800–1200)	139	55 (53–58)	BRIGHT LIMB
18 (T62)	EUV2009_285_00_23_00_UVIS_119 TI_EUVFUV001_PRIME	12 Oct	4	164.1	1285 (0–3000)	165	101 (98–102)	TWILIGHT LIMB
48 (T62)	EUV2009_285_15_19_28_UVIS_119 TI_EUVFUV002_PRIME	12 Oct	4	132.9	829 (0–2000 km)	11	91 (50–100)	AFTERNOON LIMB
60 (T62,T63)	EUV2009_315_03_12_00_UVIS_120 TI_M120R2HZ3_ISS	11 Nov	7	1354 (0–6000)	2649	118	97 (60–120)	DISTANT LIMB

from the 2009 data set were at Titan-spacecraft distance of 170,000 km or less that represents an altitude resolution of 340 km or less in the EUV and 255 km or less in the FUV in the vicinity of the airglow layer, except for F60 which is a distant limb observation at 1.4×10^6 km from Titan. This distant observation is a measurement frequently encountered during the Cassini mission. We will see that observations over 5×10^5 km are too distant to yield meaningful limb observations due to the large range of SZA and MRH included on the spectral pixels and the simultaneous inclusion of both (bright, dark) disk and limb emissions on certain pixels. All of the other observations from Figures 3a and 3b show limb spectra from either the bright or twilight or dark limb. The question remains what is the diurnal intensity variation over a period of a year for the brightest EUV and FUV features.

[17] We begin the discussion by noting that five of the spectra in Figures 3a and 3b indicate both molecular N_2 and atomic N emission features in both EUV and FUV. These observations are F0, F9, F14, F48 and F60. The EUV airglow emission spectra consistently exhibit the strong interplanetary (IP) and Titan H Lyβ atomic line, c_4' [0,1] 980 Å molecular band intensity of N_2 and N II 1085 Å multiplet. The FUV features found in the five-spectra during the same observations occur with N_2 molecular emissions for LBH and VK bands and the usual set of N I atomic multiplets (Papers 2 and 3). These features always seem to occur for solar photo-excitation for SZA < 120° and MRH near 1000 km (800–1200 km) and all Titan latitudes. The EUV emissions are strongly absorbed by CH_4 for all Titan limb observations for MRH altitudes less than 800 km. The UVIS observations depend on the FUV channel to remain optically thin below 800 km MRH until 350 km MRH over the wavelength range 1400–1900Å to allow tracking of low altitude limb airglow emissions. Magnetosphere plasma impact excitation probably occurs for F0 on the night side to account for EUV and FUV limb emissions and will be discussed in another section. We observe in Figures 3a and 3b that there are two spectra without detectable Titan–based EUV and FUV emissions. These observations are F5, and F12. F5 and F12 are dark for two reasons: 1) minimum ray heights of 2100–2600 km for F5 and 1800–2400 km for F12, both MRH sets lying above the solar and magnetosphere excited ionosphere emission altitudes of 500–1200 km and 2) a mean dark-side SZA of 143° for F5 and 100° for F12.

[18] The F18 limb spectrum is weak in the EUV (no indication of the $N_2 \, c_4'^1\sum_u^+$(0,1) band at 980 Å or N II multiplet (g ^{3}P-^{3}P^o) near 1085 Å). The FUV indicates particle scattering only, without discernible N_2 molecular bands or N I multiplets, despite containing an MRH in the ionosphere (see Figure 2). IP Lyβ (see *West et al.* [2012] for a discussion) is consistently present in all of the spectra in Figure 3a. This absence of nitrogen emission features on the limb is unusual because the FUV limb spectrum of F18 indicates particle scattering and shows that the topside ionosphere is illuminated by the solar FUV. The F18 limb pixels in the limb spectra in Figures 3a and 3b cover the range from 0 to 3000 km for all four records while the SZA is at 101° implying that the upper atmosphere at ~1000 km is in daylight. This conclusion is verified in that the FUV limb spectrum indicates a strong Rayleigh scattered component. The
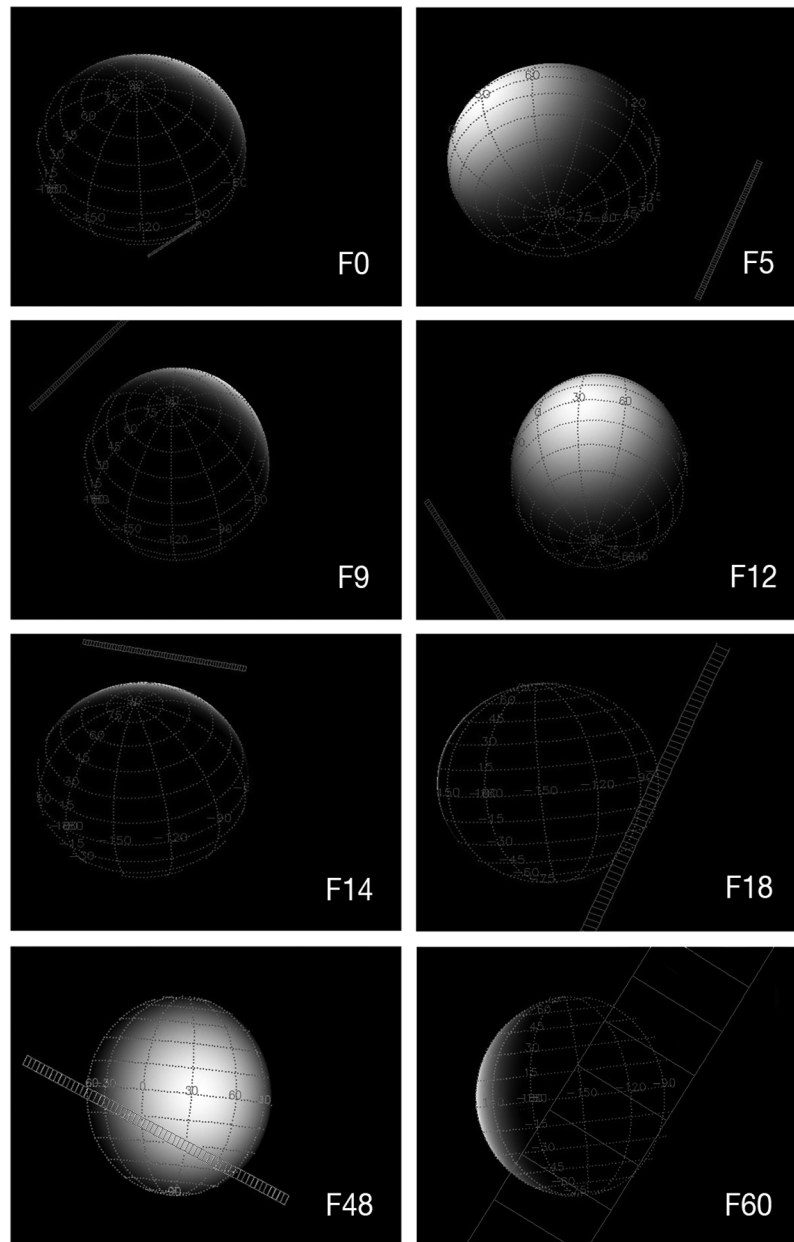
Figure 4. Geometric plots of each of the Titan limb and disk observations in 2009 by the EUV slit (2 mrad × 60 mrad) demarking the EUV and FUV UVIS spectral observations in Figures 3a and 3b limb at time of Record 0. The geometric parameters for the observation are given in the data cubes in Table 1.

VK bands (some are indicated) and weak NI FUV multiplets are observed on the twilight limb (see below) in the FUV.

[19] To continue the analysis, we note in Figure 3b that the FUV limb observations sometimes contain a long-wavelength contribution from particle scattering and solar reflection, e.g., F18, F48, and F60. The bright limb and twilight limb observations (pixels with SZA < 120°) that have a portion of the ~0.1° field of view (FOV) minimum ray height that passes through the lower thermosphere – layers 2 and 3 (300–600 km) in Figure 1 during an observation will contain this contribution as our published UVIS dayglow limb spectra as a function of altitude in *Sittler et al.* [2010a, Figure 16.24] shows. If we consider the solar generated top side airglow layer 400 km wide [800–1200 km] (Paper 3) than

a UVIS look direction toward the MRH of 800 km with a FOV of 1.5mR will include the lower thermosphere of reflecting haze at 500 km for a (closest approach) C/A distance of 150,000 km. We see why F18 and F60 include this twilight component as the C/A distance is more than 150,000 km. We use solar reflection as an important discriminator for separating twilight glow and nightglow limb observations.

[20] We consider the analysis of another important aspect of the 71 observations in 2009 by comparing intensities of the strongest EUV and FUV features over the course of the year (2009 to early 2010) at the limb regions from Figure 2: the bright limb (SZA < 90°), the twilight limb (90° < SZA < 120, and the dark limb (SZA > 120°). It is important to compare simultaneously the FUV intensities of two strong features to
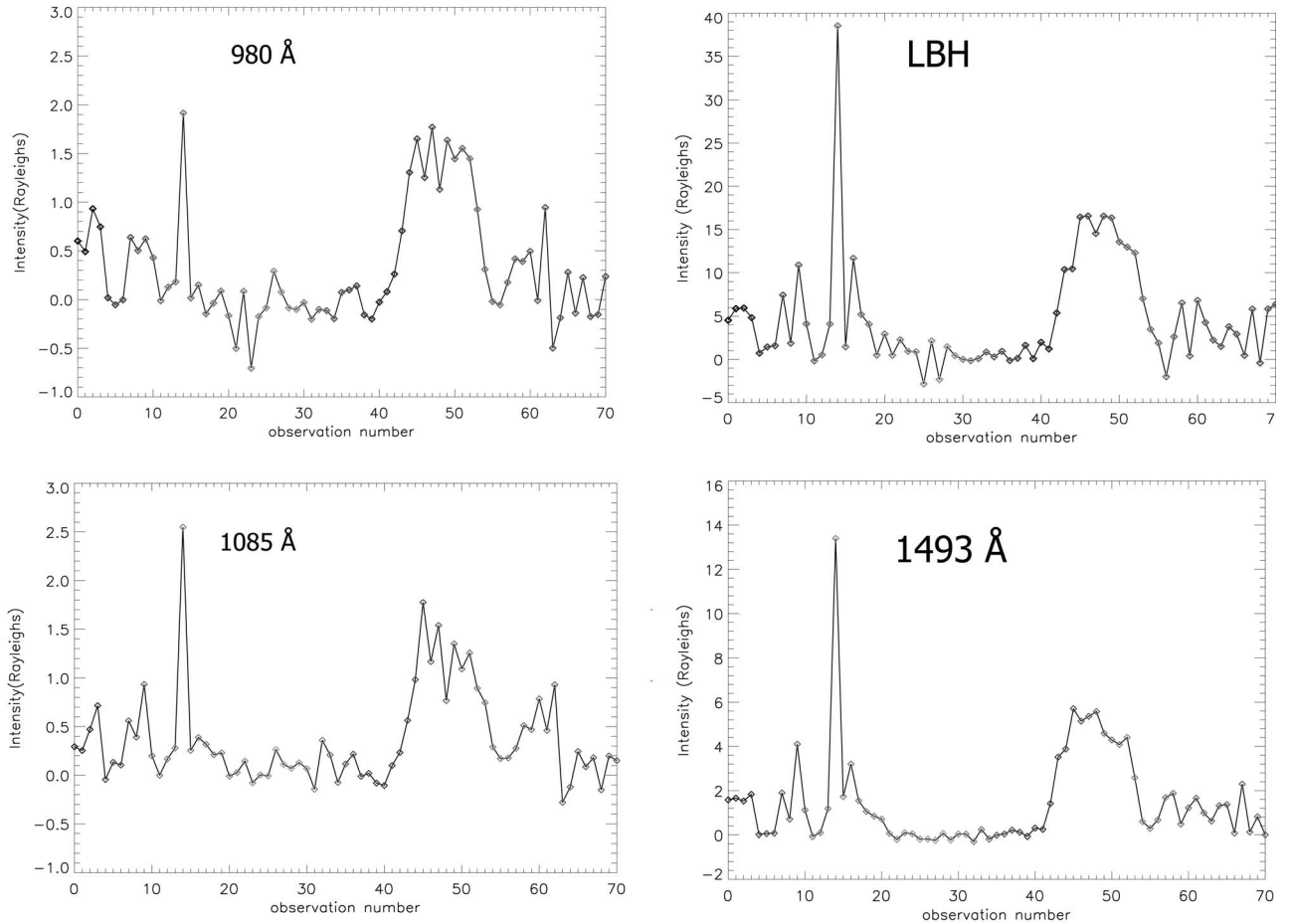
Figure 5. Mean limb intensities of EUV N II multiplet (g ^{3}P–^{3}P^o) near 1085 Å and the $c_4'(0,1)$ band at 980 Å and limb intensities of FUV N I multiplet (g ^{2}D^o–^{2}P) at 1493 Å and the LBH bands from 1300 to 1400 Å for the 71 observations of 2009 and early 2010 with the same color scheme for each observation, as defined in Figure 2. Small negative intensity numbers occur for weak emissions of some observations in the subtraction of signal minus background.

correlate emissions also generated the same way as the EUV by photoelectrons, magnetosphere plasma and PDI of N$_2$. We have shown in Papers 1 and 3 that the two brightest EUV emission features are the N II multiplet (g ^{3}P-^{3}P^o) near 1085 Å and the c_4' (0,1) band at 980 Å, both with peak limb and bright disk intensities of near 2–3 R. We have shown, in Paper 2, that two of the brightest FUV emission features are the N I multiplet (g ^{2}D^o-^{2}P) near 1493 Å and the LBH bands (a $^1\Pi_g$ – X $^1\sum_g^+$ band system) with strongest vibrational features from 1300 to 1400 Å [*Ajello et al.*, 2010, 2011a, 2011b; *Ajello and Shemansky*, 1985], both with peak limb and bright disk intensities of near 5 R and near 100 R (respectively, Papers 2 and 3). We plot for the limb the c_4' (0,1) 980 Å molecular band intensity and LBH band intensity from 1295 to 1480 Å, N II 1085Å and N I 1493Å in Figure 5. We choose N I 1493 Å, which is only secondary to NI 1200 Å in integrated intensity. The NI 1200 Å multiplet is slightly blended with Lyα at 1216 Å. We track the integrated N I, II feature intensities for the year and these features track each other nearly identically.

[21] We also show the same data again in a similar way using tabular form. From the set of 71 UVIS bright limb observations identified by data-cube name, we summarize in Table 2 the mean values of the limb intensities of the $c_4'(0,1)$ 980 Å molecular band intensity, the LBH band system intensity from 1250 to 2500 Å, N II 1085Å and N I 1493Å multiplet intensities. We distinguish the observations by the call-outs shown in Table 2 with "d" for bright limb dayglow, "t" for twilight limb and "n" for limb nightglow with an additional indication of "h" for a line-of-sight MRH that is high above ionosphere (>1500 km) and "far" for a spacecraft to Titan distance of greater than 1×10^6 km. The table is useful for separately following daylight (d), twilight (t) or nightglow (n) intensities of limb observations within the ionosphere. For example, the brightest limb observation (F14) for both atomic features occurred on 22 June 2009 with a spacecraft distance to Titan of 64,000 km and a limb "stare" MRH at 800 km (for middle pixels 30–35), SZA of 53° and TPA of 139°. Observations of the atomic features in daylight significantly above 800 km MRH (observations 7, 8, 9 in

Table 2. Limb Intensities of Brightest EUV and FUV Features

Observation	UVIS FUV File Name	Limb Intensity (Rayleighs) Airglow[a]				Notes[b]
		980 Å	1085Å	LBH	1493Å	
0	FUV2009_109_23_06_00_UVIS_109TI_FIRLMBAER001_CIRS	0.60	0.29	12.2	1.58	n
1	FUV2009_109_23_27_39_UVIS_109TI_FIRLMBAER001_CIRS	0.49	0.25	15.9	1.66	n
2	FUV2009_109_23_42_48_UVIS_109TI_FIRLMBAER001_CIRS	0.93	0.47	16.1	1.53	n
3	FUV2009_110_01_12_34_UVIS_109TI_FIRLMBAER002_CIRS	0.75	0.72	13.0	1.83	n
4	FUV2009_126_01_18_21_UVIS_110TI_EUVFUV001_PRIME	0.02	0.04	1.96	0.01	nh
5	FUV2009_126_02_11_10_UVIS_110TI_EUVFUV001_PRIME	−0.05	0.13	3.92	0.06	nh
6	FUV2009_126_03_03_59_UVIS_110TI_EUVFUV001_PRIME	0.0	0.10	4.28	0.07	nh
7	FUV2009_141_16_38_15_UVIS_111TI_EUVFUV001_PRIME	0.64	0.56	20.1	1.89	d
8	FUV2009_141_17_27_21_UVIS_111TI_EUVFUV001_PRIME	0.50	0.39	5.05	0.71	d
9	FUV2009_141_18_16_27_UVIS_111TI_EUVFUV001_PRIME	0.62	0.93	29.4	4.10	d
10	FUV2009_157_21_48_36_UVIS_112TI_EUVFUV001_PRIME	0.43	0.20	11.1	1.12	d
11	FUV2009_157_22_44_36_UVIS_112TI_EUVFUV001_PRIME	0.01	0.00	−0.46	−0.07	th
12	FUV2009_157_23_40_37_UVIS_112TI_EUVFUV001_PRIME	0.13	0.17	1.44	0.09	th
13	FUV2009_158_00_36_38_UVIS_112TI_EUVFUV001_PRIME	0.18	0.28	11.05	1.18	t
14	FUV2009_173_15_16_39_UVIS_113TI_EUVFUV003_PRIME	1.92	2.55	104.1	13.4	d
15	FUV2009_189_12_55_05_UVIS_114TI_EUVFUV002_PRIME	0.012	0.26	3.92	1.73	d
16	FUV2009_189_13_47_22_UVIS_114TI_EUVFUV002_PRIME	0.15	0.39	31.53	3.20	d
17	FUV2009_285_00_04_00_UVIS_119TI_EUVFUV001_PRIME	0.14	0.32	14..1	1.54	t
18	FUV2009_285_00_23_00_UVIS_119TI_EUVFUV001_PRIME	.04	0.21	11.0	1.05	t
19	FUV2009_285_00_42_00_UVIS_119TI_EUVFUV001_PRIME	0.09	0.23	1.36	0.85	t
20	FUV2009_285_01_01_00_UVIS_119TI_EUVFUV001_PRIME	0.16	−0.01	7.93	0.71	t
21	FUV2009_285_01_20_00_UVIS_119TI_EUVFUV001_PRIME	−0.50	0.03	1.30	0.06	th
22	FUV2009_285_01_39_00_UVIS_119TI_EUVFUV001_PRIME	0.09	0.14	6.16	−.20	th
23	FUV2009_285_01_58_00_UVIS_119TI_EUVFUV001_PRIME	−0.70	−0.08	2.52	0.09	th
24	FUV2009_285_02_17_00_UVIS_119TI_EUVFUV001_PRIME	−0.17	0.00	2.39	0.05	th
25	FUV2009_285_02_36_00_UVIS_119TI_EUVFUV001_PRIME	−0.08	−0.01	−7.65	−0.19	th
26	FUV2009_285_02_55_00_UVIS_119TI_EUVFUV001_PRIME	0.29	.27	5.78	−0.18	th
27	FUV2009_285_03_14_00_UVIS_119TI_EUVFUV001_PRIME	0.08	0.11	−6.29	0.24	th
28	FUV2009_285_03_33_00_UVIS_119TI_EUVFUV001_PRIME	−0.09	0.07	3.97	0.06	th
29	FUV2009_285_03_52_00_UVIS_119TI_EUVFUV001_PRIME	−0.10	0.13	1.19	−0.22	th
30	FUV2009_285_04_11_00_UVIS_119TI_EUVFUV001_	−0.03	0.07	0.04	0.04	th
31	FUV2009_285_04_30_00_UVIS_119TI_EUVFUV001_PRIME	−0.20	−0.14	−0.41	0.03	th
32	FUV2009_285_04_49_00_UVIS_119TI_EUVFUV001_PRIME	−0.10	0.36	0.28	−0.30	th
33	FUV2009_285_05_08_00_UVIS_119TI_EUVFUV001_PRIME	−0.12	−0.12	2.33	0.24	th
34	FUV2009_285_05_27_00_UVIS_119TI_EUVFUV001_PRIME	−0.20	−0.07	0.80	−0.18	th
35	FUV2009_285_05_46_00_UVIS_119TI_EUVFUV001_PRIME	0.08	0.12	2.55	−0.01	th
36	FUV2009_285_11_41_05_UVIS_119TI_EUVFUV002_ PRIME	0.10	0.22	−0.33	0.0	th
37	FUV2009_285_11_59_17_UVIS_119TI_EUVFUV002_PRIME	0.14	−0.01	0.38	0.21	th
38	FUV2009_285_12_17_29_UVIS_119TI_EUVFUV002_PRIME	−0.16	0.02	4.41	0.12	th
39	FUV2009_285_12_35_41_UVIS_119TI_EUVFUV002_PRIME	−0.20	−0.08	0.24	−0.07	th
40	FUV2009_285_12_53_53_UVIS_119TI_EUVFUV002_PRIME	−0.03	−0.11	5.36	0.30	th
41	FUV2009_285_13_12_05_UVIS_119TI_EUVFUV002_PRIME	0.08	0.10	3.31	0.25	th
42	FUV2009_285_13_30_17_UVIS_119TI_EUVFUV002_PRIME	0.26	0.23	14.5	1.41	d
43	FUV2009_285_13_48_28_UVIS_119TI_EUVFUV002_PRIME	0.70	0.56	28.0	3.52	d
44	FUV2009_285_14_06_40_UVIS_119TI_EUVFUV002_PRIME	1.31	0.98	28.2	3.88	d
45	FUV2009_285_14_24_52_UVIS_119TI_EUVFUV002_PRIME	1.65	1.77	44.4	5.71	d
46	FUV2009_285_14_43_04_UVIS_119TI_EUVFUV002_PRIME	1.25	1.17	44.7	5.14	d
47	FUV2009_285_15_01_16_UVIS_119TI_EUVFUV002_PRIME	1.77	1.54	39.3	5.36	d
48	FUV2009_285_15_19_28_UVIS_119TI_EUVFUV002_PRIME	1.13	0.77	44.7	5.58	d
49	FUV2009_285_15_37_40_UVIS_119TI_EUVFUV002_PRIME	1.64	1.35	44.2	4.59	d
50	FUV2009_285_15_55_52_UVIS_119TI_EUVFUV002_PRIME	1.45	1.09	36.6	4.29	d
51	FUV2009_285_16_14_04_UVIS_119TI_EUVFUV002_PRIME	1.55	1.26	35.0	4.09	d
52	FUV2009_285_16_32_16_UVIS_119TI_EUVFUV002_PRIME	1.45	0.90	33.2	4.41	d
53	FUV2009_285_16_50_29_UVIS_119TI_EUVFUV002_PRIME	0.93	0.75	19.0	2.59	d
54	FUV2009_289_15_17_59_UVIS_119TI_M90R3CLD289_ISS	0.31	0.29	9.43	0.60	far
55	FUV2009_290_04_24_59_UVIS_119TI_M90R3CLD290_ISS	−0.02	0.17	5.12	0.29	far
56	FUV2009_299_14_09_59_UVIS_120TI_M150R2HZ299_ISS	−0.05	0.18	−5.41	0.68	far
57	FUV2009_303_03_42_29_UVIS_120TI_M90R2CLD303_ISS	0.18	0.28	7.11	1.69	th
58	FUV2009_304_03_42_29_UVIS_120TI_M90R2CLD304_ISS	0.42	0.51	17.7	1.87	dh
59	FUV2009_307_13_40_59_UVIS_120TI_M90R3CLD307_ISS	0.39	0.47	1.10	0.41	far
60	FUV2009_315_03_12_00_UVIS_120TI_M120R2HZ315_ISS	0.49	0.7	18.4	1.22	th
61	FUV2009_317_20_27_59_UVIS_121TI_M90R2CLD317_ISS	−0.01	0.46	11.5	1.66	far
62	FUV2009_319_02_56_59_UVIS_121TI_M90R3CLD319_ISS	0.94	0.93	6.06	0.99	far
63	FUV2009_326_14_52_59_UVIS_121TI_M150R2HZ326_ISS	−0.50	−0.28	4.05	0.62	far
64	FUV2009_331_19_44_59_UVIS_121TI_M90R2CLD331_ISS	−0.19	0.12	10.2	1.32	far
65	FUV2009_333_01_59_00_UVIS_121TI_M90R2CLD333_ISS	0.28	0.24	7.91	1.37	far
66	FUV2009_334_21_42_04_UVIS_122TI_ECLIPSE001_ISS	−0.14	0.09	1.25	0.07	far

Table 2. (continued)

		Limb Intensity (Rayleighs) Airglow[a]				
Observation	UVIS FUV File Name	980 Å	1085Å	LBH	1493Å	Notes[b]
67	FUV2009_361_19_23_43_UVIS_123TI_FIRNADMAP001_CIRS	0.23	0.18	15.7	2.30	t
68	FUV2009_361_21_34_10_UVIS_123TI_FIRNADMAP001_CIRS	−0.17	0.15	−1.10	−0.40	th
69	FUV2010_028_18_04_24_UVIS_125TI_EUVFUV001_PRIME	−0.15	0.19	15.8	0.82	dh
70	FUV2010_028_18_31_24_UVIS_125TI_EUVFUV001_PRIME	0.24	0.15	17.2	0.00	dh

[a]Weak signals may produce a negative intensity result for (Signal + Noise) – Noise indicated in the Limb Intensity columns.
[b]Notes: d, day; t, twilight; n, night; h indicates limb observation higher than 1500 km altitude MRH; far indicates limb observations with spacecraft distance to Titan further then 10^6 km.

Figure 2) or below 800 km MRH (observations 15, 16) are weaker). Similar yearly correlations exist with the LBH band system intensity and the c'_4 (0,1) 980 Å molecular band intensity. The brightest nightglow observations occurred on F2 and F3 with a significantly greater emphasis on low altitude MRH observations of 350–800 km (to be discussed in section 4.0).

[22] The bright disk EUV observations, not shown in the figures of the 71 limb observations (we show only limb at MRH > 0 km tangent altitude), occurs on many observations with strong brightness in all these features on DOY285 F45-F52. The bright disk and limb EUV spectra of F45 - F52 are nearly as bright as F14 as shown in Figure 5. For example the brightness of 1085 Å is 2.5 Ray on F14 and is 1.5 Ray on F48. The bright limb intensities occurring on DOY285 for spacecraft-Titan distances of 120–160 k km are at similar limb distances (MRH) of approximately 1000 km of 22 June 2009 for SZA of 80–90° and a TPA of 10° (fully illuminated disk). Thus the bright limb for DOY285 was observed at a near mean 80–90° SZA. However, the distance to Titan was 132,900 km during F48 and the FOV of the FUV was 200 km, sufficiently large enough with the spacecraft motion to observe the particle scattering present from spectral contributions below 600 km, while the UVIS is pointed at the bright limb. The FWHM of the airglow layer intensities in N_2 emissions for F48 is 200–300 km. Only Titan flyby distance of 60,000 km or less, like F14, can spatially resolve the peak airglow intensity. Similarly F18 at 164,100 km with a FOV of 246 km and a SZA of 100° presented a twilight limb airglow in Figure 3b since the topside ionosphere was fully illuminated. The dark disk intensity measurements for 980 and 1085 Å are measurable on only a few observations, especially F0 and F3, and are important in deciding on the general characteristics of the nightglow intensities compared to the dayglow intensities.

3. Titan in Solar Eclipse

[23] There was a solar eclipse observation within Saturn's shadow of Titan on 7 May 2009 by UVIS from a distance of 6.43×10^5 km for record 0. The set of three eclipse observations from 2009 through 2010 are described in West et al. [2011, 2012]. In brief for the 7 May 2009 observation of the eclipse by UVIS there were 9-records (0–8) with steady viewing of 160 min (2.675 h) in Saturn's shadow. Each record was 1070 s (17.83′) in duration) and contains 60 spectra. Out of that set of 9 records there were two types of individual spectra from each record: 1) the dark disk at exact center of the pixel (e.g., EUV and FUV spatial pixels 29 to 34 indicated dark disk and were summed for each of the 9 records for a total of

54 dark disk spectra and, 2) the dark limb (FUV spatial pixels 24 to 27 and 35 to 39: a total of 90 limb spectra) accounting for the remaining spatial pixels on the dark limb. The limb pixels range in MRH values from surface to 3000 km. Most pixels outside of this set were eliminated as to be too distant from Titan to contribute to the limb spectra as each spatial pixel in the EUV accounts for a spatial resolution of 600 km. The slit-Titan (surface) geometry is shown in Figure 6 for the record 5 (0–8 total records) at the mid-time on 7 May, 09h 57′. The mid- time of record 0 was 7 May, 08h 28′, and the mid-time of record 8 was 7 May, 10h 50′. The slit was maintained in position identically for each record from 0 through 8. The spacecraft distance was so great (666,076 km for record 5) and the pointing was maintained adequately constant that only one additional pixel (each spatial pixel is 1mrad in angular FOV or 666 km in limb extent at Titan) needed to be included on the dark disk averaging with time. We included in the FUV average dark disk spectrum the average of pixel numbered 34, in the spectra from records 3, 5, 6 and 7.

[24] The spectra of dark limb and dark disk are shown in Figure 7 for the EUV: 1) in red with a data boxcar smooth of 3 for adjacent points; and 2) an nsum mathematical value of 4, which is used to obtain an average value of a single point for each group of 4 points. The EUV spectra of dark limb and dark disk are nearly identical with a similar intensity for each of the same 3 or 4 nitrogen features of peak intensities ~60 mRay/Å or about 0.2–0.5 Ray intensity for the feature for a filled field of view (FOV). The distant FOV projection on the ionosphere may be under-filled compared to the nightglow extent, since the FWHM of the ionosphere layer is roughly 400 km [Kliore et al., 2008]. The observed features are: 1) N_2 $c'_4{}^1\sum_u^+$ (3,2; 4,3) at 945 Å; 2) the N_2 $c'_4{}^1\sum_u^+$) (0,1) band at 980 Å; and 3) N II multiplet (g ^{3}P-^{3}P°) near 1085 Å. In addition, we find the interplanetary H Lyβ emission with a peak intensity of near 70 mR/Å or an integrated intensity of near 0.46 R on the limb and 0.30 R on disk, indicating the disk was blocking the infinite column extent of IP H Lyβ with the bulk of the disk emission arising from two sources: a) scattering the interplanetary glow by the eclipsed disk of Titan [West et al., 2012] and b) proton charge exchange with N_2 [Ajello et al., 2011b]. We calculate the directly observed IP H Lyβ contribution to the limb signal is about 0.16 R. The EUV nightglow features are about a factor of 5 less in intensity than the disk observations from the EUV dayglow (Paper 1) and about ten times less than limb dayglow observations (Paper 3) [West et al., 2012].

[25] We now proceed to a regression analysis of the EUV eclipse observations. The technique is explained in section 5.0, describing another set of limb observations occurring on 25 March 2008. For our eclipse analysis we choose to
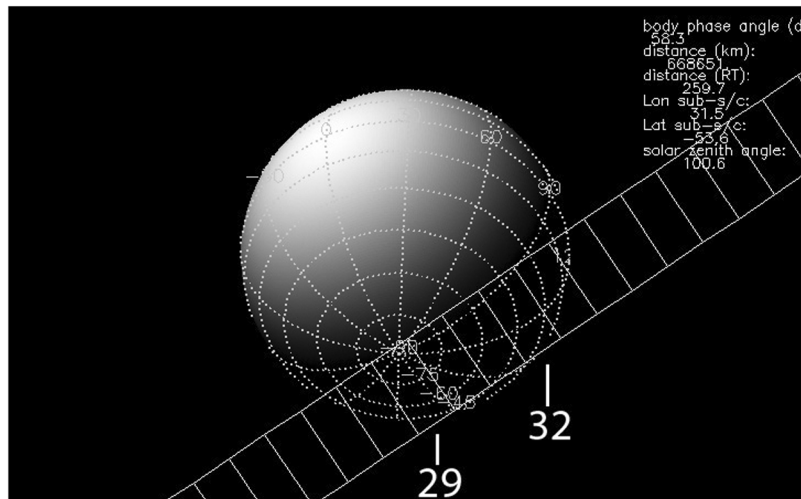
Figure 6. Geometric plot of each of the Titan limb observations during the eclipse as viewed by the Cassini UVIS slit at mid-time of Record 5 for 7 May 2009, 09^h 57′. The entire surface of Titan was in darkness. The UVIS slit is shown in the figure with the numbers 29 and 32 denoting the pixels, which are centered on the dark-disk from pixel 27 to 33. The mid-time of Record 0 was 7 May 2009, 08^h 27′, and the mid-time of record 8 was 10^h 50′. The UVIS instrument was pointed at [RA,Dec] = [200.3132, 59.6999] in degrees and is viewing northward (upwards) from Titan sub-spacecraft latitude −53.59 degrees.

combine the dark limb and dark disk data set, since many pixels are a combination of limb and disk and to allow adequate average S/N in the regression analysis. We show, in Figure 8 for the EUV, a composite regression optically thin model. The EUV spectrum is shown in Figure 8 from 900 to 1140 Å with an integrated EUV intensity of 2.0 R compared to a composite fit of 2.3 R. These intensities can be compared to a similar dayglow spectrum of 13 December 2004 analyzed by a regression analysis from 900 to 1140 Å with a measured intensity of 16.6 R and a modeled intensity of 17.5 R. For example the (Carroll-Yoshino) CY(0,1) band has a modeled eclipse intensity of 0.2 R. compared to 1.5 R in the 13 December 2004 dayglow. We see approximately a factor of 8 difference in the EUV between dayglow and nightglow intensities.

[26] The dark limb and dark disk FUV spectra (not shown) are also interesting indicating three weak nitrogen features the N I multiplets (^{4}S^o -^{4}P) at 1200 (3.1 R and 2.0 R) (^{2}D^o-^{2}D) at 1243 Å (0.94 R and 0.52 R): and (^{2}D^o-^{2}P) at 1493 Å (1.93 R and 0.55 R) on the disk and limb, respectively, and weak LBH band emissions: (3,0) at 1356 Å, (2,0) at 1383 Å and (1,1) at 1464 Å. The LBH bands, with sufficient S/N to be seen on the limb only, have a peak intensity of about 100 mR/Å per feature or an integrated intensity about 0.5 R per feature. These features represent about 5% of the band system and indicate ∼10 R emission for the LBH band system [Ajello and Shemansky, 1985]. The H Lyα intensity is 122 R on the limb and 35 R on the disk, which leads to 87 R signal intensity from IP H Lyα in the downwind direction of the interstellar wind at 20 R$_s$. Additionally, we remind ourselves that the H Lyβ IP signal is 0.16 R. We find the ratio IP H Lyα/IP H Lyβ is 544 in the downwind direction [West et al., 2012]. In comparison the New Horizons observations of the IP emissions, observes a ratio of Ly α/Ly β brightness of 600–800 (averaged over a particular 360-degree swath on the sky) [Gladstone et al.,

2012]. The intensity of H Lyα at 20 R$_s$ in the UVIS look direction shown in Figure 6 for 27 May 2009 has negligible contribution from the magnetospheric distribution of H near Saturn [Melin et al., 2009].

[27] We show in Figure 9 the regression model of the FUV eclipse spectrum from 1175 Å to 1775 Å with combined limb and dark disk pixels for S/N considerations as we performed for the EUV. The main difference between this eclipse FUV regression model and the dayglow FUV regression model lays in the fact that a solar scattering vector is not needed as the spectrum is flat and zero-level at high wavelength to 1900 Å except for very weak VK bands. The entire sphere of the moon lies in darkness. The model for the LBH bands over predicts the LBH emission rate at 19.8 R compared to an analysis of the limb spectrum, yielding 10 R as mentioned earlier. The overall model wavelength behavior is well-fit with a methane column density of 8×10^{16} cm^{-2} (column density fit by the model). The regression fit to the weak FUV eclipse signal is not sensitive to the methane column density. However, we have previously modeled the FUV spectrum of 13 December 2004 in Paper 1 and found a methane column density of 3×10^{16} cm^{-2}. Additionally, the CH$_4$ column abundance inferred from the airglow at 1000 km for T57 in Paper 3 was 2. $\times 10^{16}$ cm^{-2}, which is the formula that was used in West et al. [2012] for the analysis of the same eclipse emissions. This is about a factor of 2 less than what is reported from occultation in Shemansky et al. [2005], but it should be emphasized that the occultation experiment measures the full slant column abundance through the atmosphere whereas the CH$_4$ column retrieved from the airglow analysis is sensitive to attenuation from the tangent altitude (where the airglow is excited) to the spacecraft.

[28] The failure of the modeled intensity peaks to match the LBH and N I features at short FUV wavelengths (1200–1500 Å) may indicate proton impact mean energy with larger than 5 keV mean impact energy, producing a different
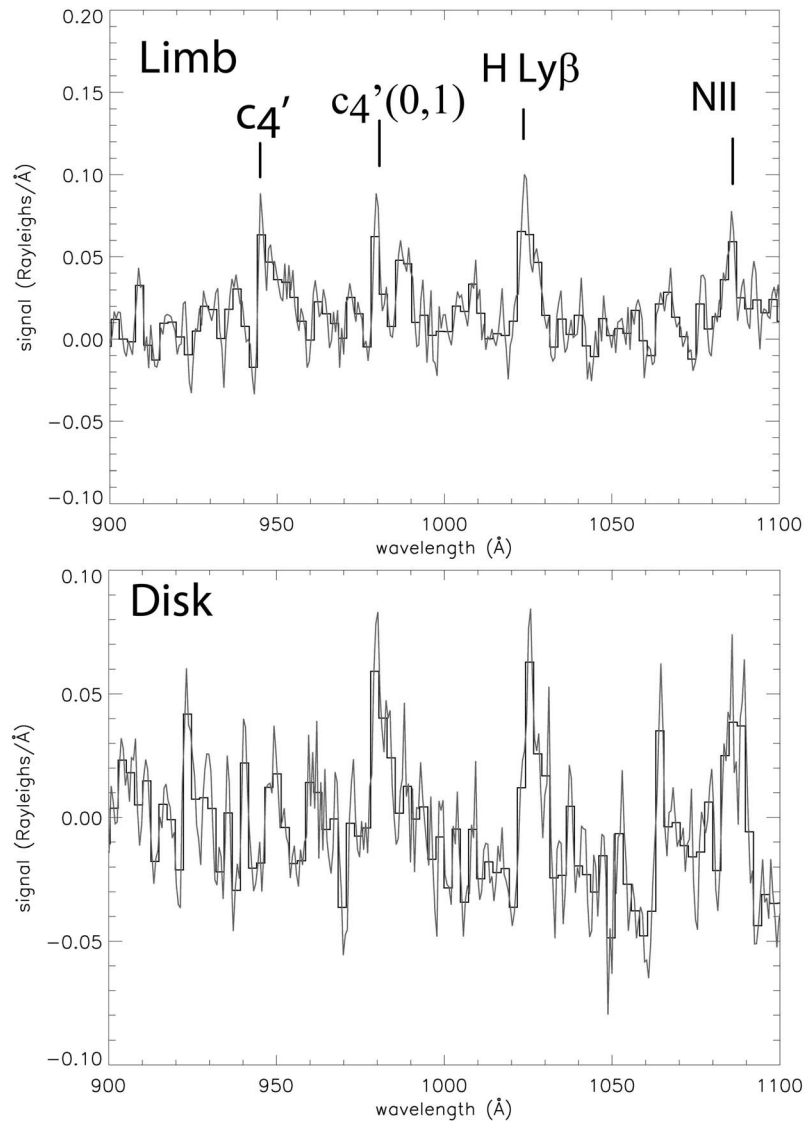
Figure 7. The EUV spectra of the limb and disk of Titan during the solar eclipse of Titan by Saturn. The strong emission features of $c_4'\,^1\Sigma_u^+(v'=0) \to X(v''=1)$ at 980 Å, H Ly β at 1025 Å, N II (1085 Å) are indicated in both limb and disk. The limb spectrum also shows the blended $c_4'\,^1\Sigma_u^+(v'=4,3) \to X(v''=3,\,2)$ molecular bands near 945 Å. The EUV spectra are smoothed by 3-pixels in red, and the nsum data = 4 (average sum of 4 pixels per point) is shown in black in the histogram mode.

relative set of intensities than measured in our laboratory. It is also possible that having different impacting species (such as H_2^+, He^+ and water group ions-O^+, OH^+) will influence these ratios [*Sittler et al.*, 2010a]. As for electrons, the LBH relative band intensities are expected to closely follow Franck-Condon factors at all energies except for collisional cascade from the a′ and w-states [*Ajello et al.*, 2010, 2011a]. The total eclipse intensity for the combined limb and disk data is 130 R of which 115 R arises from disk + limb H Lyα. The composite intensity for the entire wavelength range found at this modeling stage is 172 R, which is 25% too large to match the data. We find the eclipse data is not of sufficient spatial resolution to distinguish limb and disk or to guarantee a filled FOV for the pixels chosen as we can assure from other nightside observations at much closer distance as described in section 4.0.

[29] Let us consider the data on strong atomic lines from EUV and FUV dark disk and limb spectra individually. There are strong spectral features of H Lyα (1216 Å) and H Lyβ (1025 Å) in the FUV and EUV, principally from interplanetary H solar fluorescence on the limb and from Titan reflection of interplanetary hydrogen on the dark disk. The FUV H Lyα intensity is 122 R on the dark limb and 32 R on the dark disk, after subtracting the contribution from N I 1200 Å from the wings of H Lyα. These numbers can be directly compared to calculation from a model presented in *West et al.* [2012]. West *et al.* find an intensity of 23 R from reflection of interplanetary H Lyα by the dark disk of Titan with an uncertainty of a factor of two, indicating an intensity range of 12R to 46 R. The remaining emission of $9 \pm\,^{11}_{\,9}$ R from dark disk may be produced by charge exchange with impacting protons, a strong excitation process of Lyα observed in the
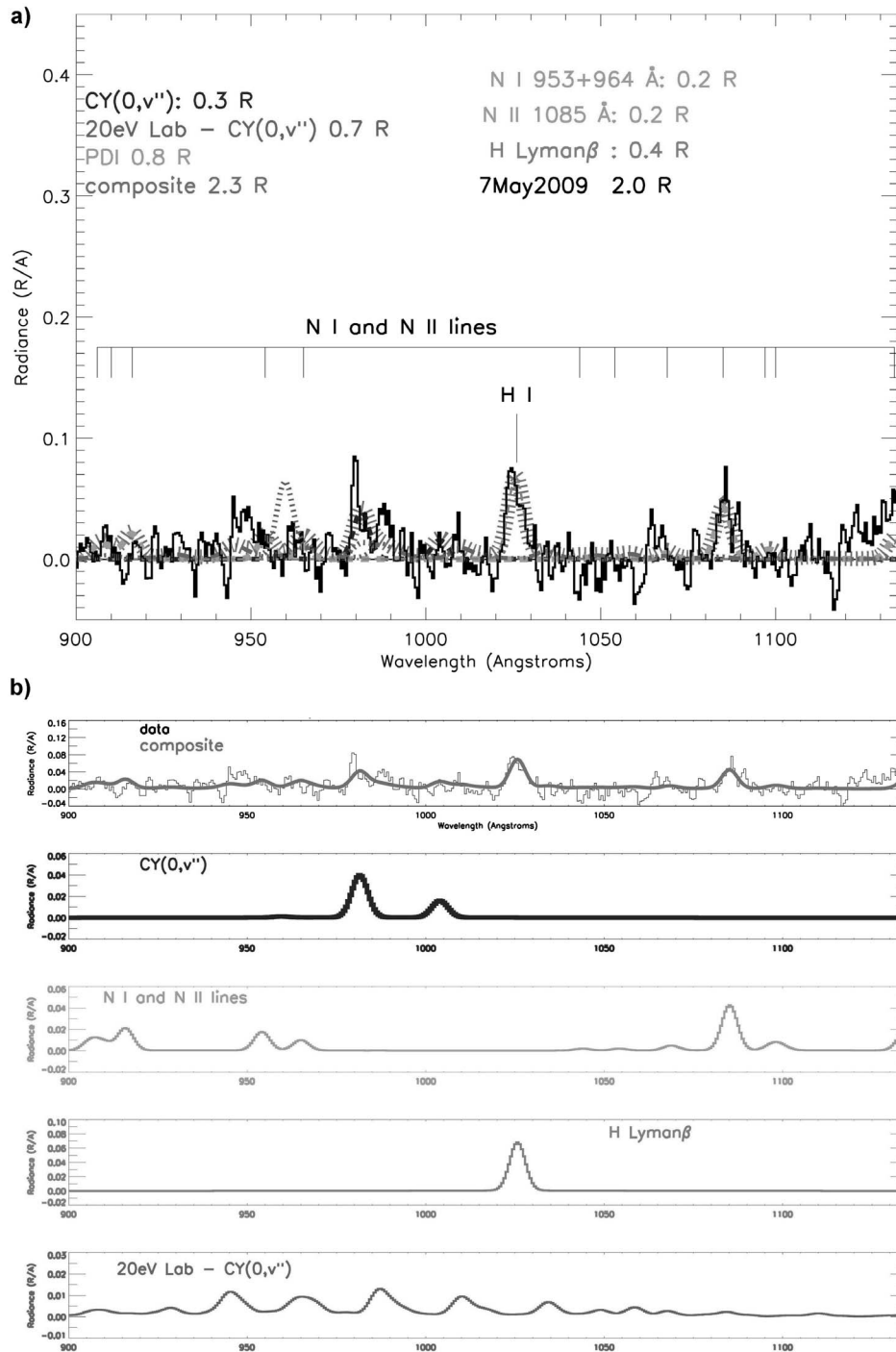
Figure 8. (a) Regression model fit to UVIS EUV eclipse spectrum (black with smooth of 3-pixels) from 7 May 2009. The composite model (orange) includes four independent vectors (totals indicated; see text). We designate: 1) green for the CY (0, v″ = 0, 1, 2)]; 2) light blue for the NI and NII lines; 3) dark blue for the H Lyβ feature near 1026 Å; and 4) red for the N_2 RV bands based on a 20 eV laboratory spectrum. The optically thin $c_4'(0) \rightarrow X(0)$ band that was removed from vector 1 (20 eV spectrum) is shown in dotted-light green, and the loss in area of the $c_4'(0,0)$ band represents multiple-scattering predissociation of N_2. (b) The composite model fit to the data, followed by the four individual model fits to the UVIS data for each vector. The individual panels are: 1) data in black and composite model fit orange; 2) the CY bands for v′ = 0,v″ = 0.1; 3) the NI,II lines in same PDI ratios as in *Stevens et al.* [2011]; 4) Lyman-β; and 5) the RV bands of N_2 at 20 eV from electron impact measured in the laboratory. The strongest are b $^1\Pi_u$, b′ $^1\Sigma_u^+, c_4'$ $^1\Sigma_u^+ \rightarrow X^1\Sigma_g^+$.
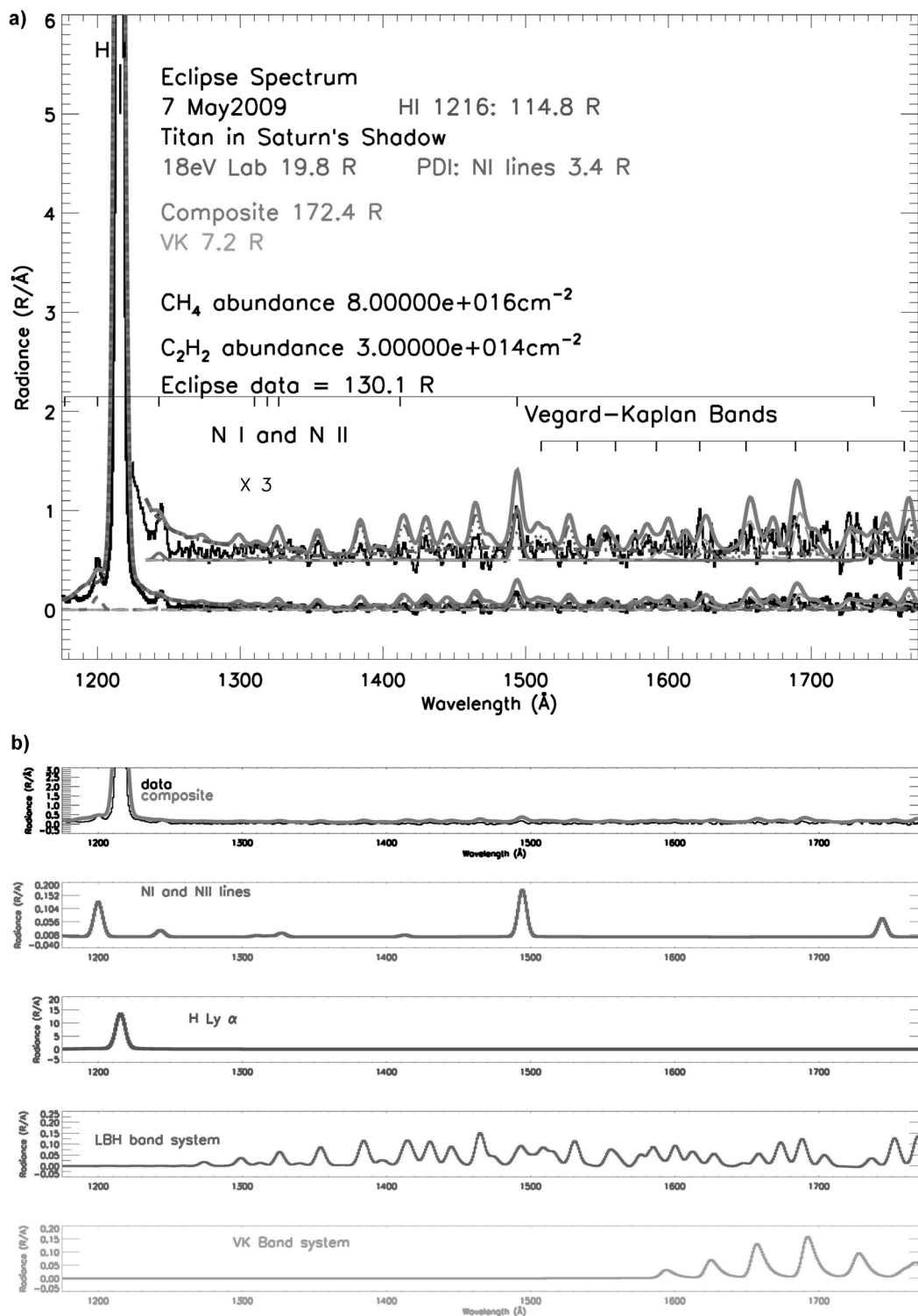
a)

Eclipse Spectrum
7 May 2009   HI 1216: 114.8 R
Titan in Saturn's Shadow
18eV Lab 19.8 R   PDI: NI lines 3.4 R

Composite 172.4 R
VK 7.2 R

CH_4 abundance $8.00000e+016 cm^{-2}$

C_2H_2 abundance $3.00000e+014 cm^{-2}$

Eclipse data = 130.1 R

N I and N II

X 3

Vegard–Kaplan Bands

b)

data
composite

NI and NII lines

H Ly α

LBH band system

VK Band system

Figure 9. (a) Regression model fit (orange) to the FUV eclipse spectrum (black) from 7 May 2009 in black (smooth of 3-pixels). The composite model (orange) includes four independent vectors (totals indicated; see text). We designate: 1) red for the LBH spectrum); 2) purple for the NI and NII lines; 3) green for the H Ly-α feature near 1216 Å; and 4) light blue for the N_2 VK bands based on a model spectrum [Stevens et al., 2011]. (b) The data composite regression (orange) fit to the data (black) in the first panel followed by four panels of individual modeling vectors. The regression model (orange) in the first panel includes: 1) N I spectrum from dissociative ionization (same ratios as PDI) of N_2 in purple in the second panel; 2) the H Lyα feature at 1216 Å in green in the third panel; 4) the LBH 20 eV laboratory spectrum in red in the fourth panel; and 5) the VK band system in light blue in the fifth panel.

laboratory [*Ajello et al.*, 2011b] and possibly a small amount also from interplanetary H Lyα along the line of sight from the spacecraft to Titan. A discussion of the wide range of uncertainty in the contribution to the H Lyα signal from charge exchange is given in West *et al.* [2012].

[30] The ratios of N I 1200 Å/N I 1493 Å (including some contribution from the LBH bands at 1493 Å) may be indicative of characteristic of either electron impact induced fluorescence or proton induced fluorescence of N_2. These laboratory-based optically thin ratios are similar and have been found to be 2.4 for electron impact excitation at 100 eV [*Ajello and Shemansky*, 1985] and 2.0 for proton induced fluorescence at 5 keV [*Ajello et al.*, 2011b]. The energy dependence of atomic line ratios from electron dissociative processes are typically found to be constant to about 20% [*Ajello and Shemansky*, 1985; *Ajello and Franklin*, 1985]. The measured emission line multiplet ratios are ∼3 on the limb (3.10 R/1.03 R) and disk (1.99 R/0.64 R). The published N I 1200 Å/N I 1493 Å limb and disk observations with a ratio near 2 (Papers 1 and 3) were affected by CH_4 absorption. We consider this ratio again in another dark side observation 30 times closer to Titan in section 4.

4. Observations of the Lower Atmosphere Below 1000 km MRH

[31] We show in Figure 10 (bottom) the geometry for the Titan observation in F3 at time of record 0 and record 1 with the EUV slit nearly perpendicular to the limb. The start time of record 0 occurs at 20 April 2099 at 1^h 09′ 8″ and the start time of record 1 was exactly 4′ later at 1^h 13′ 8″. The slit image is continuously moving as the UVIS slit pans higher into the upper atmosphere with time. The EUV spectrum of F3 for the dark limb is shown for record 1 (top) and the FUV spectrum for record 0 (middle) on 2009-DOY110 of Figure 10. The F3 observation took place at a closer range distance of the spacecraft to Titan than the other 70 Cassini spacecraft observations. F3 acquired four records of Titan at spacecraft distances of 15,557 km, 16827 km, 18,106 km and 19,392 km representing a factor of ∼30–40 closer than the eclipse, ensuring a filled FOV for each pixel of either the disk or limb. The F3 EUV observation was composed of four 4-min records. We selected record 0 and record 1 for discussion in the FUV and EUV, respectively, since the UVIS slit shown in Figure 10 (bottom) remains partially on the Titan disk and lower atmosphere for the first two records only. We follow upon the discussion with a regression analysis of record 1 for both the EUV and FUV. The orientation of the slit is such that pixel 0 is at the highest altitude and pixel 59 is on the surface (below disk). The relative spacecraft motion moves both the UVIS slits swiftly upwards through the upper atmosphere of Titan from 556 to 818 km for pixel 0 of record 0 and from 818 km to 1111 km for the four minutes of record 1. Numerically larger pixel numbers are at lower attitudes with pixel 33 on the surface-tangent at the start of record 0 and with pixel 46 on the surface-tangent at the start of record 1. We choose to use only a subset of the 60 spatial pixels of the slit for record 1 that remain on the dark disk or dark limb for the entire 4 min, pixels 57 to 59 for the disk (S/N is insufficient for dark disk regression analysis but indicates same spectral features as the limb) and pixels 0 to

44 for the dark limb. The EUV signal for dark limb observations are strong on all four records throughout the thermosphere region with MRH from 300 to 1500 km. The limb SZA's for F3 record 0 and 1 are about 123°, indicating that the topside ionosphere (∼1200 km) is in darkness from solar XUV. We very carefully calculated the shadow heights for every pixel element on record 0 and 1. We find, for the F3 observation, that the sun's light will not illuminate any portion of Titan's atmosphere below 4000 km along the Cassini line of sight for either the EUV field of view (FOV) with an opaque altitude of 800 km or the far FUV FOV with an opaque altitude of 350 km, since the shadow height altitude remains above 4000 km for all 60 pixels at their respective MRH values. The region from 800–1500 km, representing the topside ionosphere, is in darkness, and the observed EUV spectra mainly derive excitation from plasma impact.

[32] We will further analyze record 1 limb spectrum. The emission MRH altitudes for the limb spectra of record 1 observed by the EUV UVIS spans most of the entire ionosphere from grazing the surface at 0 km for pixel 42 at the start of record 1 to 797 km for pixel 0 and completing record 1 at 1089 km for pixel 0 at the end of 4 min. We have constructed for the F3 an average dark limb spectrum spanning the ionosphere. The Titan atmosphere will transmit to Cassini UVIS EUV limb spectra from the MRH altitude for pixel line-of-sight (LOS) distances above 800 km. Thus the spectra arising from MRH altitudes below 800 km will contain line-of-sight (LOS) spectra from volume elements of spherical shells of the atmosphere above 800 km altitude. The EUV darkside limb spectrum of record 1 (shown in Figure 10, top) is smoothed by seven pixel elements and shows about 8 identifiable features with peak emission rates at the limb of ∼0.1 R/Å at about of 25% of the peak EUV intensity emission rate of ∼0.4 R/Å for the same spectral features observed for the dayglow limb observation of 22 June 2009, F14, at 800–1000 km and about twice the intensity of the eclipse EUV observation shown in Figure 8. Figure 10 shows the following emission features: N II(^{3}P←^{3}P^o) at 916 Å, c'_4(3,2; 4,3) at 943 Å, N I(^{4}S^o←^{4}P) at 954 Å, c'_4(0,1) at 980 Å, c'_4(0,2) at 1003 Å, H Ly β at 1025 Å, N II(^{3}P←^{3}D^o) at 1086 Å and N I(^{4}S^o←^{4}P) at 1134 Å.

[33] Similarly, we show in Figure 10 (middle) the F3 FUV spectrum of record 0 (smoothed by 7 pixels for improved S/N) for the dark limb over-plotted with a laboratory proton-excited LBH spectrum and a model VK spectrum. Once again we use only a subset of the 60 spatial pixels of the FUV slit for record 0 choosing pixels that remain on the dark limb for the entire 4 min, pixels 0–32 for the limb. The vertical resolution of the FUV and EUV spatial pixels are less than 50 km. The FUV limb spectrum clearly shows both LBH and VK band system vibrational features with a spectral intensity about of 20% of the intense dayglow limb observation of F14. The brighter LBH features have a peak intensity of ∼0.3 R/Å versus ∼1.5 R/Å on F14 (and versus 0.1 R/Å during the eclipse). The H Lyα FUV signal from limb and disk are nearly identical with intensities of 40 R on the limb and 36 R on the disk, indicating that on F3 the H Lyα comes mainly from Titan atmosphere scattering of interplanetary Lyα [*West et al.*, 2012]. The H Lyα disk and limb intensities of F3 are nearly the same, and similar to the disk observation of the eclipse.
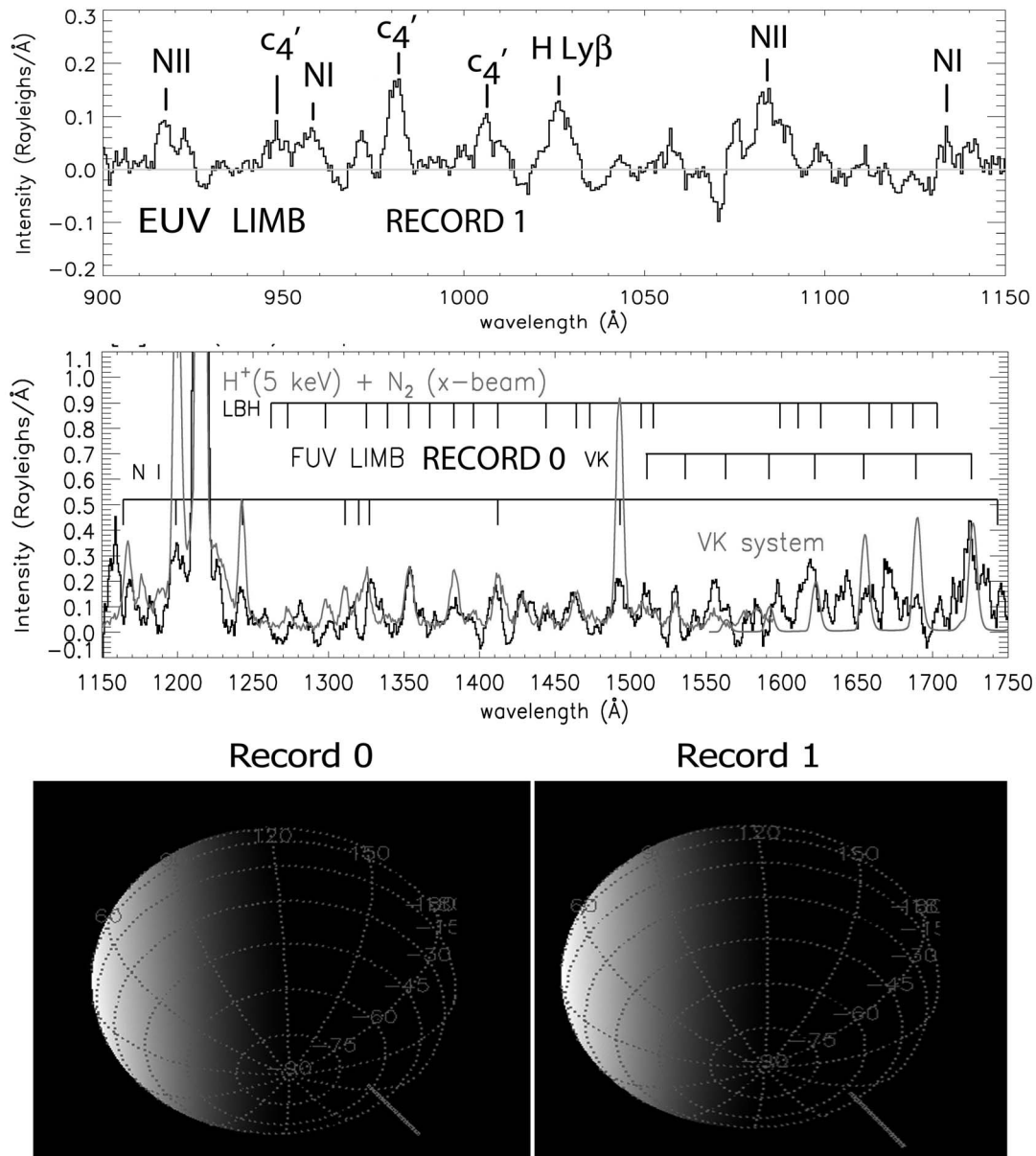
EUV2009_110_01_12_34_UVIS_109TI_FIRLMBAER002_CIRS

Figure 10. (top) The EUV spectrum of F3 from Record 1 (smooth = 7) is shown for dark limb (pixels 0–45), which is from data cube EUV 2009_110_01_15_34_UVIS_109TI_FIRLMBAER002_CIRS_750_800.sav. The strong features are identified by tick mark positions of NII (917 Å), N_2 $c_4'^1\Sigma_u^\mp$ (v' = 4, 3) → X(v'' = 3, 2) at 945 Å, N I (953 Å), $c_4'^1\Sigma_u^+$ (v' = 0) → X(v'' = 1) at 980 Å, $c_4'^1\Sigma_u^+$ (v' = 0) → X(v'' = 2) at 1003 Å H Lyβ at 1025 Å, N II (1085 Å), and N I 1134 Å. (middle) The FUV spectrum (black) of observation F3 for the dark limb for record 0, which is FUV2009_109_23_06_00_UVIS_109-TI_FIRLMBAER001_CIRS_750_800.sav. Record 0 pixels that are on the limb for the full four minutes are 0–32. The overplot in green is a laboratory spectrum of 5 keV proton excited N_2 showing the LBH bands, H Lyα and the N I multiplets. The overplot in orange shows the electron excited synthetic model spectrum of the VK bands of N_2. (bottom) The geometry of the UVIS observation of F3 for the initial time of Record 0 and Record 1 that starts on 2009_DOY110_01^h_09'_08" for Record 0 at an initial distance of 14925 km and at 2009_DOY110_01^h_13'_08" for Record 1 at an initial distance of 16,190 km for the 4-min data records. The location of the slit is near the south pole at about 58°S.

[34] There is additional evidence that the FUV Record 0 signals for LBH band features and atomic multiplet wavelengths below 1400 Å arise from a higher and different altitude than the 1493 Å multiplet. The ratio of the NI 1200 Å/NI 1493 Å integrated intensities are close to 1.5 as the NI 1200 Å mutiplet is weakened at deep layers below 800 km by CH_4 absorption.

[35] We have over-plotted the Titan FUV UVIS spectrum in Figure 10 (middle) with our recent optically thin laboratory FUV proton-induced fluorescence spectrum in green of p(5 keV) + N_2 illustrating strong LBH bands [Ajello et al., 2011b]. Proton impact on N_2 molecules to depths of 500–600 km has been modeled by Cravens et al. [2008, 2009]. Our 5 keV proton impact laboratory spectrum reasonably matches the Titan FUV spectrum for most peaks from 1100 to 1600 Å and in the laboratory the H Lyα arises mainly from a charge transfer reaction (or electron capture reaction) with N_2. We also show the synthetic spectrum of electron induced fluorescence of the VK bands referenced in Paper 3; this marginal match is well-improved in the regression analysis to follow with a smooth of the data by 3-pixels.

[36] As for the eclipse observation, we now proceed to a regression analysis of the F3 limb observation for record 1 with a smooth of the data by three. We show a limb spectrum for record 1 in Figure 11 for the EUV and in Figure 12 for the FUV. Both data sets are well-matched by a composite regression model. The EUV spectrum is shown in Figure 11 from 900 to 1150 Å with an integrated EUV intensity of 5.5 R compares to a composite fit of 5.0 R. These intensities can also be compared to a similar dayglow spectrum of 13 December 2004 analyzed by a regression analysis from 900 to 1140 Å with a measured intensity of 16.6 R and a modeled intensity of 17.5 R. For example the CY(0,1) band has a modeled F3 intensity of 0.9 R. compared to 1.5 R in the 13 December 2004 and 22 June 2009 dayglow (and about 4-times the intensity of the eclipse observation). We see approximately a factor of ∼2–5 differences in the EUV between dayglow and F3 nightglow atomic and molecular intensities. For example, the N II 1085 Å intensity in F3 was 0.7 R compared to 3.9 R on 22 June 2009 and 2.3 R on 13 December 2004. This nightglow spectrum appears to be at least a factor of two brighter than the eclipse spectrum, but the weakness of the eclipse spectrum could be partially due to the filling factor. The importance of the filling factor in the eclipse observations is thoroughly discussed in West et al. [2012].

[37] We show in Figure 14 the regression model of the FUV F3 spectrum from 1175 Å to 1775 Å. The main difference between F3 FUV regression model and the eclipse FUV regression model lies in fact that a weak solar scattering vector is useful in the F3 regression model and may arise from multiple scattering around the moon from the bright disk hemisphere as the Cassini LOS within the thermosphere and exobase region is in darkness. The chi squared regression factor is slightly improved including this weak vector addition in the regression model. It is difficult to choose between the two models (with and without solar scattering) that only differ in the amount of VK emission intensity. The model for the LBH bands predicts the LBH emission rate at 20.1 R and for the VK bands the model projects an emission rate of 2.6 R (9.6 R without long wavelength solar scattering). Stevens et al. [2011] find a peak LBH dayglow intensity of 136 R and a VK dayglow intensity of 67.8 R for F14.

We find an LBH intensity of 43 R in Paper 1 for the 13 December 2004 observation. Taken together, these dayglow changes indicate significant variations in the FUV dayglow for all atomic and molecular emissions, as Figure 5 already demonstrates for the 71 observations considered.

[38] The atomic lines in the FUV dayglow as in the EUV dayglow are about a factor of five stronger than the F3 nightglow intensities. The F3 intensity of atomic N I 1200 Å is 2.9 R compared to an intensity of 1.5 R for N I 1493 Å. The ratio of a factor of two for the intensities of N I 1200 Å/N I 1493 Å is the same ratio as found by Stevens et al. [2011] in the dayglow from the fluorescent emission attributed to electron impact reduced by the effect of CH_4 absorption. The F3 ratio is more characteristic of proton impact as measured in the laboratory by Ajello et al. [2011b]. The overall regression model wavelength behavior is well fit with a methane column density of 2×10^{16} cm^{-2}. The absorption cross section of methane is nominally 2×10^{-17} cm^2 in the FUV at 1200 Å, indicating only a small 10% absorption slant transmission effect to match the F3 EUV observation that occurs at about 900 km altitude on Titan, a representative mean altitude for the F3 EUV and FUV spectra [Cravens et al., 2009]. The total F3 integrated intensity for the data is 113.2 R, which can be broken down using the model: 1) 59 R arises from H Lyα (including the broad wings shown in Figure 14, top) and 2) 21.5 R from long FUV wavelength multiple solar scattering to the dark side. The composite intensity for the entire wavelength range found at this modeling stage is 124 R, which well-matched the composite data intensity.

[39] The main difference between F0 (another close encounter darkside observation from a spacecraft to Titan distance of 19,970–23,866 km) is a weaker airglow FUV spectrum of limb than F3 (and F14) (∼1/2 (∼1/10) of the intensity of EUV and FUV airglow spectrum of F3 (F14)). We note also that the F0 disk observation positions the UVIS slit near the equator (8°–20°S) and F3 is more polar 45°–60°S. The EUV limb airglow spectrum of F0 is equally intense as F3 is for the limb (compare Figures 3a and 5 with Figure 9).

[40] The latitude location of the F3 EUV and FUV emissions are similar to the near-polar latitude found by Kliore et al. [2008] for the strong lower altitude sporadic layer of peak electron density layer near 500 km from a radio occultation measurement on orbits T12 and T14. The latter radio occultation occurs with southern polar latitudes nearly the same as the UVIS F3 observation location [Cravens et al., 2009].

[41] The ISS photometric filtered image [West et al., 2011, 2012] indicated circum-Titan plasma particle excitation of a nightglow producing the 300–1100 nm visible-optical-near IR spectra with maximum intensity on a line from Titan to the sun through the Saturn disk. We have possibly identified the spectral features from our laboratory work on N_2 electron impact fluorescence [Mangina et al., 2011]. The laboratory spectrum from 2000 to 11,000 Å is identified as molecular emission bands of the First Positive Band System (1PB) $B\ ^3\Pi_g^+(v') \rightarrow A\ ^3\sum_g^+ (v'')$ and the Second Positive Band System (2PB) $C\ ^3\Pi_u (v') \rightarrow B\ ^3\Pi_g (v'')$ of N_2, the First Negative Band System (1NB) $B\ ^2\sum_u^+ (v') \rightarrow X\ ^2\sum_g^+ (v'')$ and Meinel Band System (MB) $A\ ^2\Pi_u (v') \rightarrow X\ ^2\sum_g^+ (v'')$ of N_2^+ ions, as well as line emissions of N (N I) and N$^+$ (N II) in the Visible-Optical-near IR.
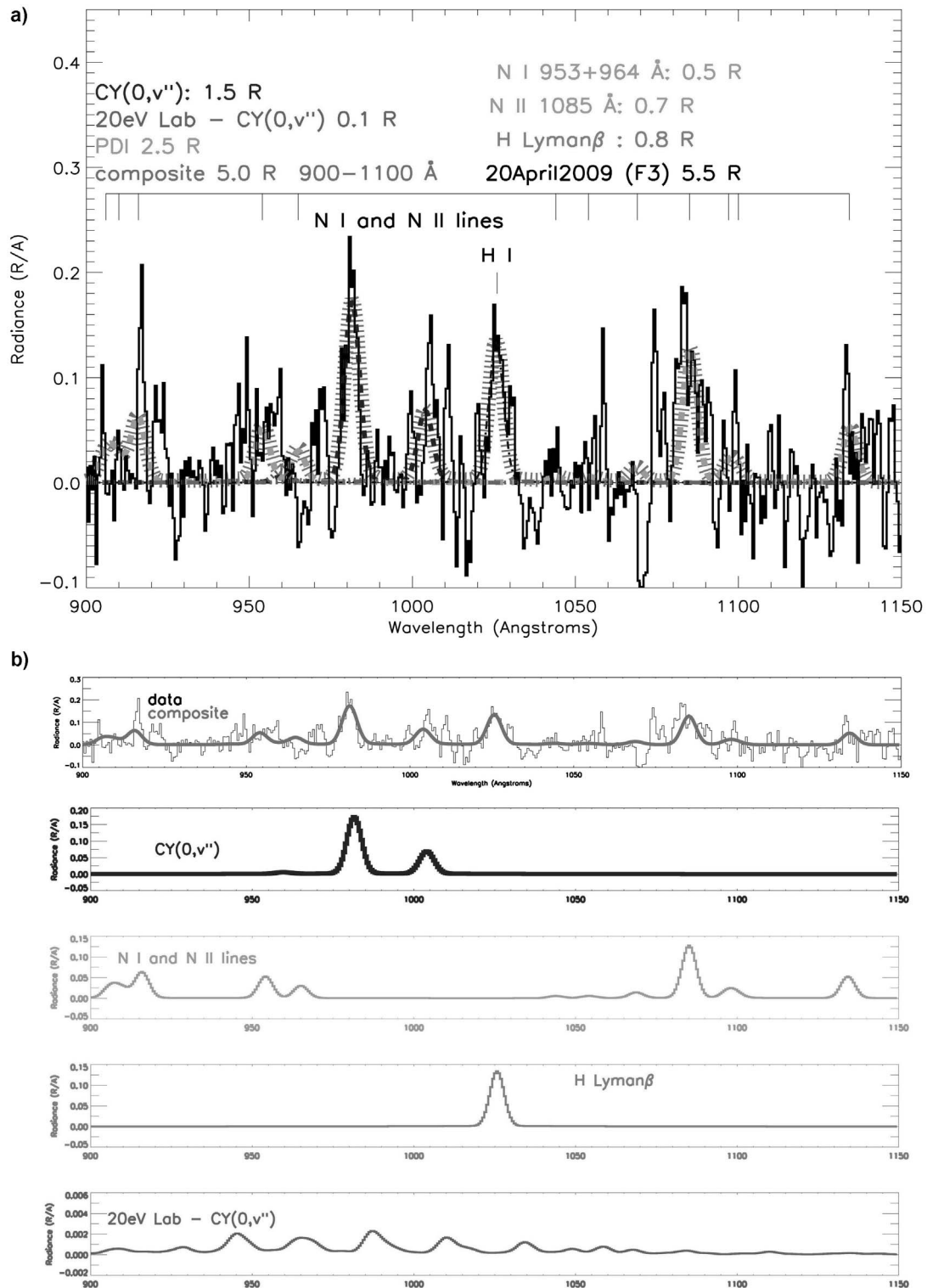
Figure 11. (a) Regression model fit to UVIS EUV F3 Record 1 limb spectrum (black, smooth is 3-pixels) from 20 April 2009. The composite regression model (orange) includes four independent vectors (total integrated intensity indicated for each vector; see text). (b) The composite model fit (orange) to the data (black) followed by the four individual fits to each vector. The individual panels are: 1) data in black and composite model fit in orange in the first panel; 2) the CY bands for $v' = 0$, $v'' = 0, 1, 2$ in green in the second panel; 3) the N I,II lines in same PDI ratios as in *Stevens et al.* [2011] in light blue in the third panel; 4) Lyman-β in dark blue in the fourth panel; and 5) the RV bands of N_2 at 20 eV from electron impact measured in the laboratory b $^1\Pi_u$, b' $^1\Sigma$, c $^1\Sigma \rightarrow X$ $^1\Sigma$ in red in the fifth panel.
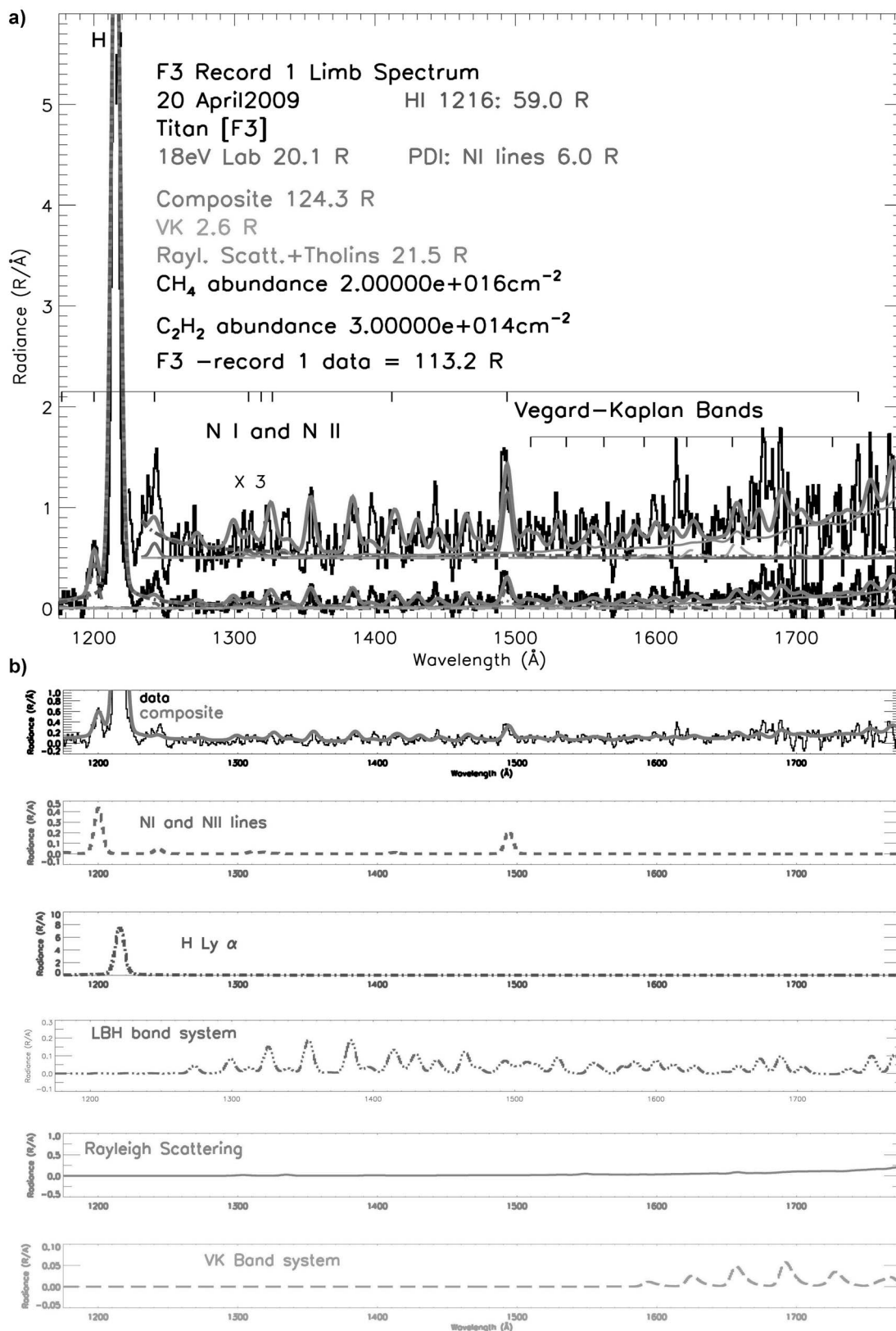
a)

F3 Record 1 Limb Spectrum
20 April2009   HI 1216: 59.0 R
Titan [F3]
18eV Lab 20.1 R   PDI: NI lines 6.0 R

Composite 124.3 R
VK 2.6 R
Rayl. Scatt.+Tholins 21.5 R
CH$_4$ abundance 2.00000e+016cm^{-2}

C$_2$H$_2$ abundance 3.00000e+014cm^{-2}

F3 −record 1 data = 113.2 R

N I and N II

X 3

Vegard−Kaplan Bands

H

Radiance (R/Å)

Wavelength (Å)

b)

data
composite

NI and NII lines

H Ly α

LBH band system

Rayleigh Scattering

VK Band system

Figure 12

[42] Energetic protons and oxygen ions have been observed in Saturn's outer magnetosphere and can precipitate into Titan's atmosphere where they deposit energy, ionize, and drive ionosphere chemistry. Ion production rates caused by this precipitation have been calculated using fluxes of incident 27 keV to 4 MeV protons measured by the Cassini MIMI Instrument [*Cravens et al.*, 2008]. These authors find that significant ion production rates exist in the 500 km to 1000 km altitude range. This is the MRH altitude range of Record 0 and Record 1 where the UVIS observes significant EUV and FUV night airglow emissions for F0 and F3. The FUV instrument has a sharp transmission decrease below wavelengths of 1400 Å at 700 km vertical height for disk viewing and 800 km MRH vertical height for slant transmission limb observations. The FUV limb spectrum is optically thin for CH_4 absorption for all altitudes (above 350 km) and above a wavelength of 1400 Å. We surmise that the UV airglow spectra in Figure 11 and Figure 12 arise from all MRH altitudes either above 350 or above 800 km depending on spectral wavelength (see shadow-height discussion in sections 1 and 5).

5. Regression Model of 25 March 2008 UVIS Observation

[43] The 25 March 2008 UVIS EUV observation of Titan from a distance of 260,671 km and target phase angle of 111.6° is shown with slit location in Figure 13 for the mid-time of record 0. All the 60 pixels of the FOV of both the UVIS slits simultaneously contain either the bright limb, bright disk, dark disk or the dark limb. We have an opportunity to analyze the average spectrum for each of these spectral pixel sets, separately. For that purpose, we also show in Figure 13 (bottom) the integrated intensity signal for all 60 spatial pixels and 20 records for several key emissions: H Ly α, NI 1494 Å and the particle scattering, the latter over the wavelength range from 1520 to 1910 Å. It appears that the radius of the planet is different for each emission, since the limb altitude (pixel) for peak signal depends on wavelength. The smallest altitude ($\sim$0–200 km above the surface) occurs for the haze producing the particle scattering in the long wavelength range of the FUV. The next altitude profile shown is the airglow layer from N_2 PDI and secondary electron ionization-excitation near 1000 km, and finally the H Ly α emission profile near the exobase at 1400 km. We also note that though the disk surface is in darkness in Figure 13 (bottom), that the upper atmosphere is catching some sun light at the maximum SZA of $\sim$115°. We see secondary minima in each of the three emission features near the dark side limb and continue to denote this lighting condition as atmospheric twilight. The 25 March 2008 observations provide verification of the importance of different

shadow height calculations for the different FUV wavelength ranges.

[44] First, we analyzed the two EUV spectra for the bright limb and the bright disk (not shown). In Figure 14 we show the EUV spectra for the dark limb and dark disk. Each of these spectra were analyzed according to regression models of N_2 emission spectra as presented in Papers 1 and 2, using the Jet Propulsion laboratory (JPL) laboratory e + N_2 18 eV spectrum (with the CY(0, v″ = 0, 1, 2) bands removed), a spectrum too low in impact energy to contain N I, II multiplets. This modeling technique is the same approach as Papers 1 and 2 and a different approach than in Paper 3 where the different features arising from either photoelectron excitation or photo-fragmentation were fit separately. The optically thin 18 eV electron impact laboratory fluorescence spectrum (simulating the airglow spectrum of the N_2 bands) was measured at 0.5 Å FWHM with the ad hoc removal of the optically thick c′(0, v″ = 0–2) progression, which dominates the optically thin laboratory spectrum (in orange in dots) in the regression model in Figure 14.

[45] The EUV dark limb and dark spectra are fit between 850 and 1150 Å and all of the features are convolved with the UVIS instrument line shape before inclusion into the least-squares fitting algorithm. The different spectral components are listed below:

[46] 1) *The CY(0, v″) bands*. The (0,0) and (0,1) bands near 958 and 980 Å, respectively, are fit together but we use the (0,1)/(0,0) ratio of 40 calculated under limb viewing conditions from a multiple scattering model [*Stevens*, 2001], thereby rendering negligible the contribution from the optically thick (0,0), as observed [*Ajello et al.*, 2007]. The (0,2) band near 1003 Å is fit separately and the (0, v″ > 2) bands are weak and are part of the 18 eV laboratory spectrum used as the main fitting spectrum for the regression analysis (Paper 1).

[47] 2) *The strong dipole-allowed transitions of N_2 in the EUV*. The electronic transitions proceed from the X $^1\Sigma_g^+$ ground-state to several closely spaced ($\sim$12–15 eV) RV states, which are the source of the molecular emissions in the EUV observed by spacecraft and have recently been studied in our laboratory at medium-to-high spectral resolution ($\lambda = 0.1$ Å FWHM). The 18 eV laboratory spectrum in the regression model contain optically thin emissions from these three states to the ground state, except for most transitions terminating in v″ = 0, which are lost to multiple scattering. Other electronic states contribute weaker emission bands found in the EUV spectrum (Ajello et al., submitted manuscript).

[48] 3) *Excess of CY(v′ = 3, 4, 6) bands as found in Paper 3*. Since the vibrational features are relatively weak and blended, all three of these progressions are fitted together as one spectral component using the relative cross sections of

Figure 12. (a) Regression model fit to the UVIS FUV F3 Record 1 limb spectrum (black, smooth is 3-pixels) from 20 April 2009 in black. The composite model (orange) includes four independent vectors (totals indicated; see text). We designate: 1) red for the LBH spectrum; 2) purple for the N I and N II lines; 3) green for the H Lyβ feature near 1026 Å; and 4) light blue for the N_2 VK bands based on a model spectrum [*Stevens et al.*, 2011]. (b) The data composite regression (orange) fit to the data (black) in the first panel followed by five panels of individual modeling vectors. The regression model (orange) in the first panel includes: 1) N I spectrum from dissociative ionization (same ratios as PDI) of N2 in purple in the second panel; 2) the H Lyα feature at 1216 Å in green in the third panel; 3) the LBH 20 eV laboratory spectrum in red in the fourth panel; 4) the Rayleigh scattered component described in the fifth panel in dark blue; and 5) the VK band system in light blue in the sixth panel.
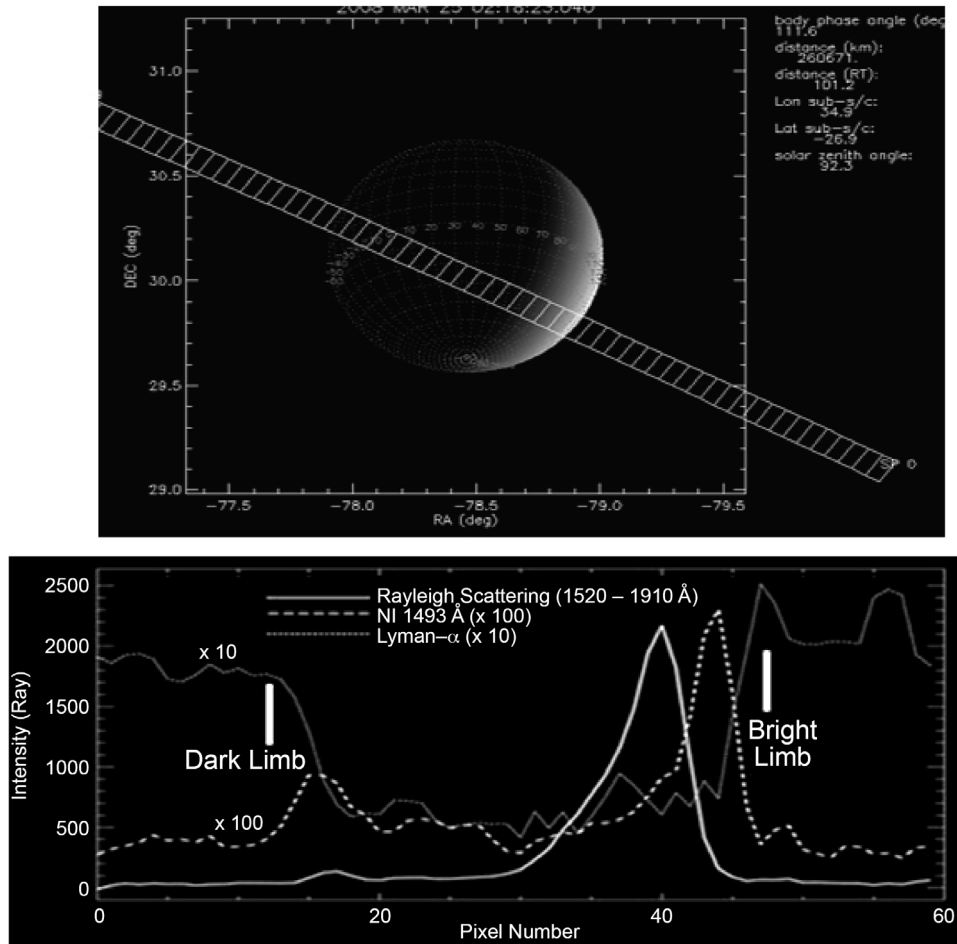
Figure 13. (top) Geometric plot of the Titan 25 March 2008 observation as viewed by the Cassini UVIS EUV slit at mid-time of Record 0. The UTC mid-time of Record 0 was 25 March 2008, 02^{h}18′. There were twenty 4.5-min records. (bottom) The integrated intensity signal for each of 60 spatial pixels summed over 20 records for key emissions: H Ly α, NI 1494 Å and the particle scattering, the latter over the wavelength range from 1520 to 1910 Å.

Ajello et al. [1989, 1998; submitted manuscript, 2012]. To a good approximation the ratio of rotational-vibrational cross sections is independent of electron energy, for electron energies distant from threshold by ∼5–20 eV. The ratio of relative emission intensities are mainly dependent on the ratio of perturbed emission transition-probabilities for the Rydberg-valence states of N_2 [*Liu et al.*, 2005, 2008; *Ajello et al.*, 1989], which are independent of electron energy, since the CY bands are not populated by cascade.

[49] 4) *N I and N II multiplets.* These features are produced primarily by photo-fragmentation of N_2. There are a total of 16 atomic multiplets within the UVIS EUV spectral region. The brightest three atomic features as measured in the laboratory under optically thin conditions are fit individually: N II 1085 Å, N I 1134 Å and N II 916 Å. The other 13 atomic multiplets in the EUV from 862 Å to 1100 Å are fit as one spectral component according to the laboratory-measured relative intensities of *Samson et al.* [1991].

[50] 5) *The H Lyman-β line at 1026 Å.* The brightest EUV (850–1150 Å) spectrum (not shown) arises from the bright limb with an observed intensity of 22.4 R compared

to the bright disk intensity of 10.9 R (half as much as the bright limb). The dark side spectra (850–1150 Å) are also about half the brightness with a measured limb brightness of 11.0 R and a measured dark disk brightness of 6.2 R indicated in Figure 14. We believe the dark side spectra for 25 March 2008 arise from a fully illuminated ionosphere at 1000 km (800–1200 km layer profile) altitude. To illustrate this point we show in Figure 15 an over plot of two disk spectra in both the EUV and FUV. The first spectrum in Figure 15 in each channel is in black and represents a disk spectrum in the range of 90–110° SZA (100° in plot caption) called a dark disk spectrum versus a second spectrum disk spectrum in range 110°–130° (120° in plot caption) also called a dark disk spectrum. The two disk spectra are nearly identical in intensity.

[51] The starting point for the regression fitting procedure in the FUV requires fitting the particle scattering vector in the 1500–1880A region to get the mixing ratios of C_2H_2, haze, C_2H_4 and C_4H_2. We find the mixing ratios of hydrocarbons relative to N_2 to be: 3.9×10^{-6} for C_2H_2, 9.7×10^{-8} for C_2H_4, ∼0 for C_4H_2 and 9.8×10^{-11} for haze, exactly as we
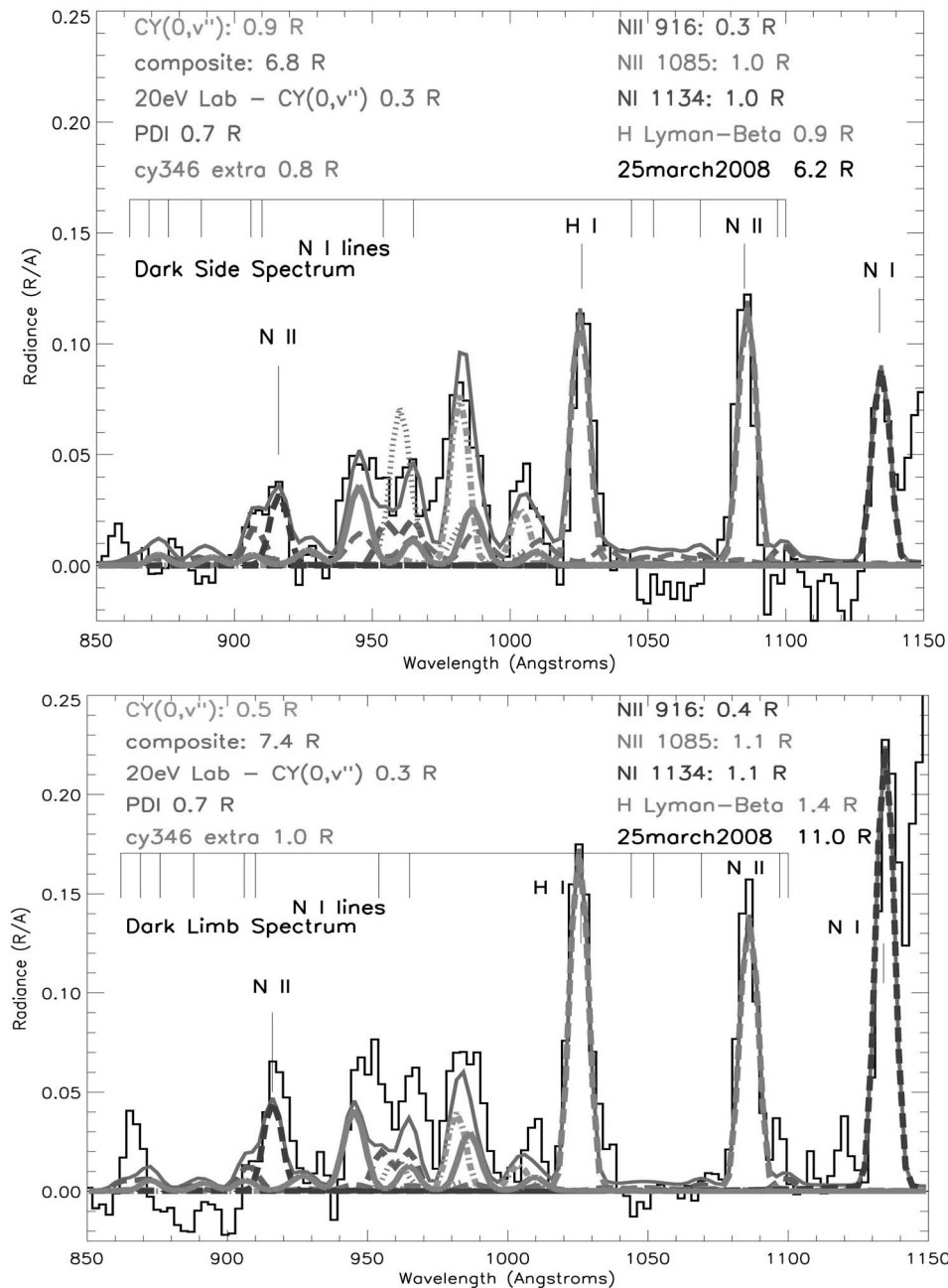
Figure 14. (top) Model fit to UVIS dark side limb EUV spectrum (black) from 25 March 2008. The regression model composite fit (solid green) includes seven independent vectors (totals indicated by color; see text). The optically thin $c'_4(0) \rightarrow X(0)$ laboratory band that was removed from vector 1 of CY bands (laboratory 20 eV spectrum) is shown in dotted-yellow and is replaced by a model described in Papers 1 and 3. The optically thick $c'_4(0) \rightarrow X(v'' = 0, 1, \ldots)$ bands are calculated as described in the text (Papers 1 and 3) and are in blue, and the loss in area of the $c'_4(0,0)$ band contributes multiple-scattering predissociation of N_2. The optically thin laboratory spectrum (orange) was used to model the remainder of the N_2 electronic band systems which are optically thin; the atomic lines are modeled in green, yellow and blue as described in Paper 3 [see also *Samson et al.*, 1991; *Meier et al.*, 1991; *Bishop and Feldman.*, 2003; *Bishop et al.*, 2007]; and the CY $v' = 3$, 4, 6 bands in purple are modeled as described in Paper 3. (bottom) Dark limb data and regression model as in Figure 14 (top).

did in Paper 2. In Paper 2 we found similar mixing ratios of hydrocarbons relative to N_2 to be: 2.4×10^{-6} for C_2H_2, 5.7×10^{-8} for C_2H_4, 1.2×10^{-8} for C_4H_2. Our abundance ratios sample all the altitudes above 300 km, i.e., the altitudes

where the reflected solar flux is contributing to the FUV Titan spectrum [*Wilson and Atreya*, 2004]. Moreover, each individual FUV pixel probes all the layers that cross along the line of sight. The retrieved mixing ratio thus cannot
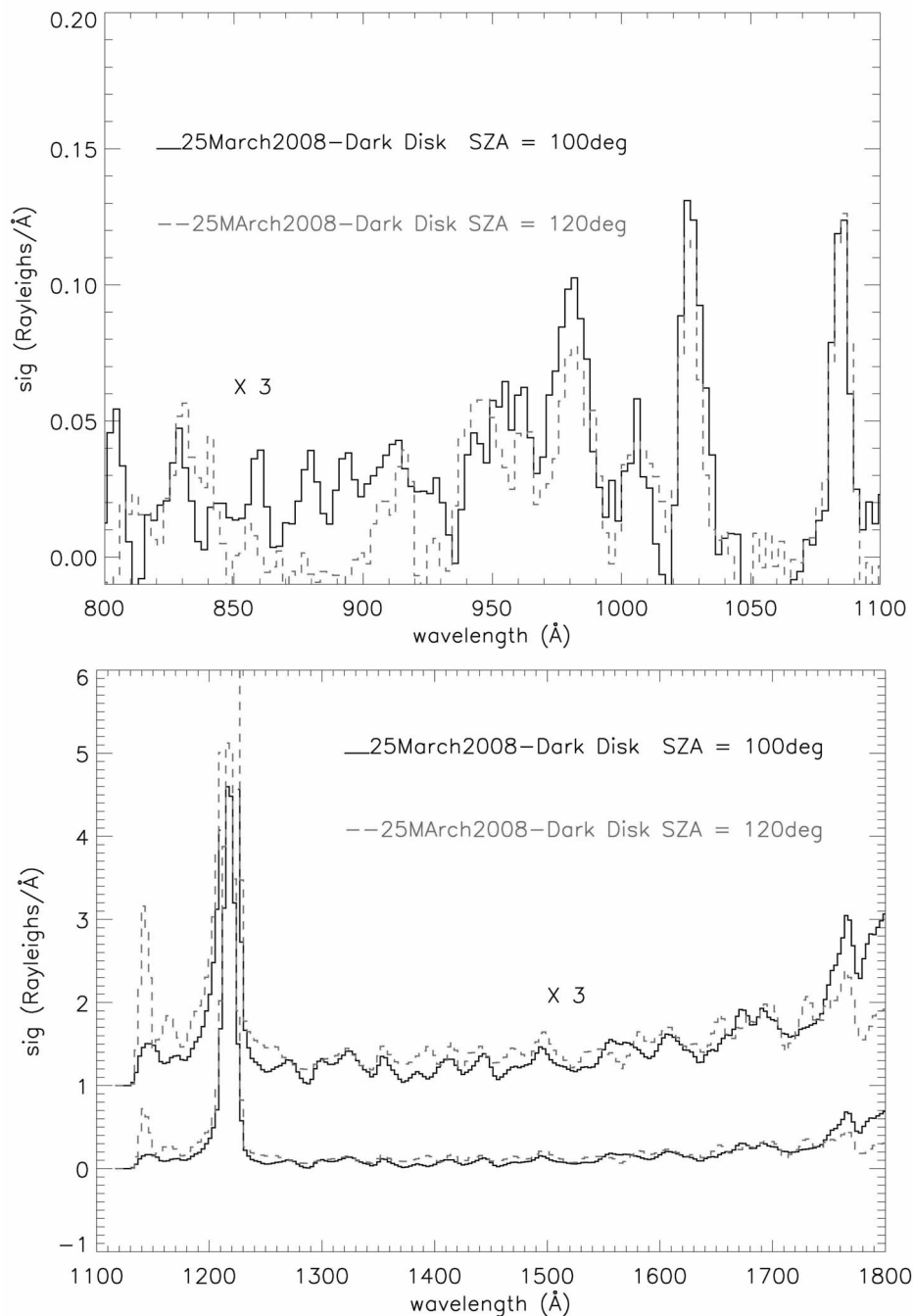
Figure 15. (top) The EUV disk spectrum from 25 March 2008 at 100° (90–110°) SZA (black) and 120 (110–130°) SZA (dash-orange). (bottom) The FUV disk spectrum from 25 March 2008 at 100° SZA (black) and 120° SZA (dash-orange).

be readily compared to other measurements. A significant latitudinal variability has also been noted by *Vinatier et al.* [2007], which makes the comparison even more difficult.

[52] We then use these mixing ratios with absorption cross sections to derive the reflected sunlight for the whole UVIS band pass. We used a TIMED SEE solar spectrum from 2008 DOY87 [*Lean et al.*, 2011; *Kameta et al.*, 2002]. The sun that day at earth orbit is the same as that which was seen by Titan on DOY 085. The regression fits, as described earlier, to the FUV spectra for the twilight disk and twilight

limb are shown in Figure 16. The spectra contain solar scattering at a low level compared to bright disk and bright limb (not shown).

6. Summary

[53] The 1-yr set of observations, studied in this work, occurred mostly in 2009 and allow varied geometry e.g., the spacecraft distances to Titan change from 10^4 to 10^6 km, the MRH values vary from 0 to 7000 km, the SZA values vary
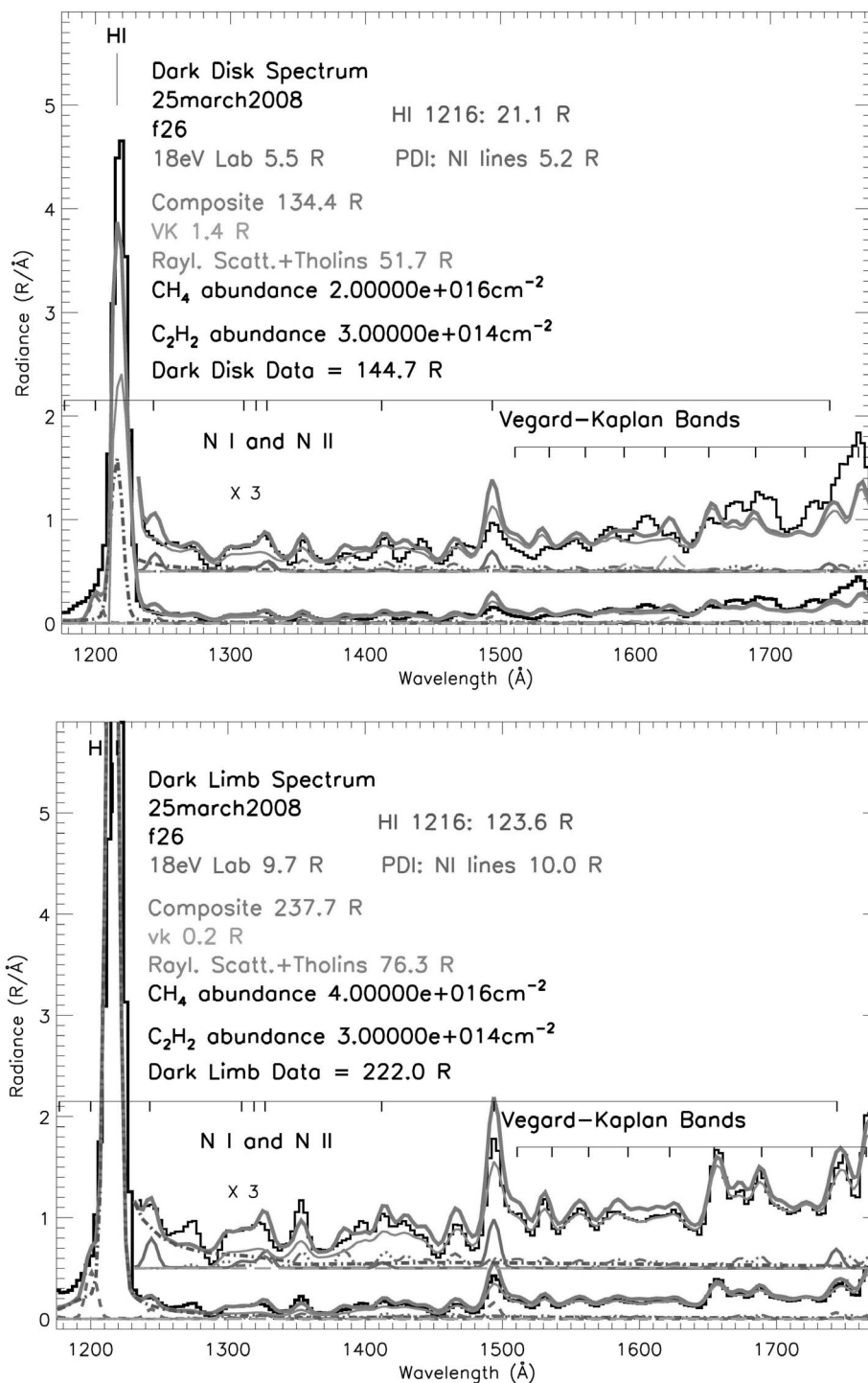
Figure 16. (top) Regression model fit to the FUV twilight glow disk spectrum from 25 Mar 2008 from 1175 to 1775 Å with a particle scattering model described in Paper 2. The model used a TIMED SEE solar spectrum from 2008 DOY87 for the solar reflection component. The regression model (orange) includes four independent spectra: 1) LBH spectrum in red (see text); 2) PDI spectrum from dissociative ionization of N_2 in purple; 3) the Rayleigh scattered component described in Figure 15 in blue; and 4) the H Lyα feature at 1216 Å in green. (bottom) Twilight glow data and regression model as in Figure 16 (top). The modeling parameters for C_2H_2 and CH_4 column densities are shown. The spectral component intensities of the four independent variables and composite spectrum are listed.

from 50° to 150°. The altitude of peak UV emission on the limb of Titan during daylight occurred inside the thermosphere at the altitude of the ionosphere (near 1000 km altitude). This altitude layer has a sunset into total darkness at ~120° SZA.

[54] The 71 airglow observations analyzed in this paper show EUV (600–1150 Å) and FUV (1150–1900 Å) atomic multiplet lines and band emissions arising from photoelectron induced fluorescence and solar photo-fragmentation of molecular nitrogen (N_2) during the dayglow (SZA < 90°) and twilight glow (90° < SZA < 120°). We also have identified similar but weaker nightglow emission (SZA > 120°) for the first time on Titan from magnetosphere plasma impact on the N_2 atmosphere. A "stare" dayglow observation on 22 June 2009 at 800–1200 km with SZA of 53° MRH produced the highest S/N spectrum with the peak airglow region approximately 200 km FWHM in width in altitude. There is a twilight glow that persists with solar depression angle for 30° past the terminator, until the solar XUV shadow height passes the highest altitude of the topside ionosphere near 1200 km. The twilight FUV and EUV spectra are similar to the dayglow spectra but weaker in intensity by a factor of about two. The nightglow spectra are weaker yet by a factor of 3–10 from the dayglow intensities.

[55] The F3 polar nightglow limb observation (20 April 2009) integrated EUV and FUV intensities are about 1/3 the dayglow intensity of the 13 December 2004 and 22 June 2009 observations and appears to be brighter than the F0 equatorial nightglow spectra in the EUV (see Figure 5). More information about the nightglow spectra is obtained by reviewing the 71 observations studied in 2009. The first four data points of Figures 2 and 5, representing F0 though F3 low-altitude (<1000 km mean MRH altitudes) LOS observations (Titan encounter T53), indicate nightglow spectra with prominent band and atomic line emission intensities shown in Figure 5. The data points of band and line intensities indicate that F3 was the brightest on the average in the EUV of the four nightglow observations and that the four observations measured FUV intensities that are similar, at least for the LBH bands and the NI 1493 Å. Figure 5 shows that F3 was about twice as bright as F0 in the EUV. Also a more interesting perspective is that Figure 5 shows that the LBH intensity and 1493 Å intensity of F14 (22 June 2009) are about 7–8 times brighter than the corresponding F3 or F0 intensities, while in the EUV F14 the N_2 $c_4'^1\Sigma_u^+$ (0,1) band at 980 Å, and the N II multiplet (g ^{3}P-^{3}Pᵒ) near 1085 Å are only three times brighter than the corresponding intensities in F3.

[56] Beyond 120° SZA, when the upper atmosphere of the moon is in total darkness, there are UV emissions from plasma impact of charged particles [Cravens et al., 2008] over an extended altitude from 500 to 1200 km. The weak emissions are variable and occur at about 10–20% of the level of the dayglow. First in the EUV at the distance of 600,000 km as in the eclipse, we perceive three strong features in the EUV: the c_4'(0,1) band at 980 Å, the H Lyβ line at 1025 Å, the N II 1085 Å multiplet in the EUV and several N I multiplets at 1200 Å, 1243 Å and 1493 Å with a weak N_2 LBH band system in the FUV. However, at the closest approach Titan-spacecraft distance of F0 and F3 (~20,000 km) of T53 we see additional strong features in the EUV and FUV with filled FOV for each pixel. We find the c_4' (3,2) and c_4' (4,3)

bands at 945 Å, the c_4'(0,2) band at 1003 Å, the N I multiplet at 1134 Å and the N II 917 Å multiplet. These features are difficult to see in the weak eclipse spectrum. In the FUV we find the VK and LBH bands. The latter emission set particularly the VK system and the NI 1493 Å multiplet appears to be excited from below 800 km limb ray height to a level originating from lower thermosphere, mesosphere, haze layer extending downward to ~500 km. These emissions possibly result from proton- and/or heavier ion-induced emissions as well as secondary-electron-induced emissions. The depth of penetration is consistent with the models of *Wilson and Atreya* [2004] that show particle impact becomes important below 1000 km, providing an important source in the lower ionosphere region.

[57] The eclipse observations are unique and have been reported in a recent pair of publications [*West et al.*, 2011, 2012]. UV emissions were observed during only one of the three eclipse events, and only weak LBH and Vegard-Kaplan (VK) emissions were seen in the FUV. The F0 and F3 observations show the advantage of the close-encounter and low altitude MRH 500–1000 km for high S/N observations for Titan dark side measurements of the FUV emissions of the VK and LBH band systems. Near-polar observations may be more intense in the UV as a complementary result to strong polar lower atmosphere electron density profiles as illustrated by *Cravens et al.* [2009] and *Kliore et al.* [2008]. The darkest (no particle scattering) FUV limb and disk spectra that include a UV slant path contribution from the lower ionosphere layer occur during the 7 May 2009 eclipse. These UV eclipse spectra, which show low signal intensity, will be useful in putting an upper limit to the role of magnetosphere plasma excitation.

[58] We have employed regression analysis using laboratory spectra of the 25 March 2008 UVIS Titan observation, which included four types of measurements (bright and dark disk and bright and dark (twilight) limb); and we have analyzed the intensities and identified each spectral feature from the limb or disk emission spectrum. The N I multiplets, N_2 VK and N_2 LBH bands are prominent in the twilight glow until 120° SZA. The details of the spectral content are given in Papers 2 and 3. We plan further work to model magnetosphere plasma energy input to the nighttime airglow emissions.

References

Ajello, J. M., and B. Franklin (1985), A study of the extreme ultraviolet spectrum of O_2 by electron impact, *J. Chem. Phys.*, *82*, 2519, doi:10.1063/1.448301.

Ajello, J. M., and D. E. Shemansky (1985), A reexamination of important N_2 cross sections by electron impact with application to the dayglow: The Lyman-Birge-Hopfield band system and N I (119.99 nm), *J. Geophys. Res.*, *90*, 9845–9861, doi:10.1029/JA090iA10p09845.

Ajello, J. M., C. W. Hord, C. A. Barth, A. I. Stewart, and A. L. Lane (1973), Mariner 9 Ultraviolet Spectrometer Experiment: Afternoon terminator observations of Mars, *J. Geophys. Res.*, *78*(20), 4279–4290, doi:10.1029/JB078i020p04279.

Ajello, J. A., G. K. James, B. O. Franklin, and D. E. Shemansky (1989), Medium-resolution studies of extreme ultraviolet emission from N_2 by electron impact: Vibrational perturbations and cross sections of the $c_4'^1\Sigma_u^+$ and $b'^1\Sigma_u^+$ states, *Phys. Rev. A*, 40, 3524–3556, doi:10.1103/PhysRevA.40.3524.

Ajello, J. M., G. K. James, and M. Ciocca (1998), High-resolution EUV emission spectroscopy of the N_2 c′ $^1\Sigma_u^+$ v′ = 3 and 4 levels by electron impact, *J. Phys. B At. Mol. Opt. Phys.*, 31, 2437–2448, doi:10.1088/0953-4075/31/10/028.

Ajello, J. M., et al. (2007), Titan airglow spectra from Cassini Ultraviolet Imaging Spectrograph (UVIS): EUV analyses, *Geophys. Res. Lett.*, 34, L24204, doi:10.1029/2007GL031555.

Ajello, J. M., et al. (2008), Titan airglow spectra from the Cassini Ultraviolet Imaging Spectrograph: FUV disk analysis, *Geophys. Res. Lett.*, 35, L06102, doi:10.1029/2007GL032315.

Ajello, J. M., R. S. Mangina, and R. R. Meier (2010), UV molecular spectroscopy from electron impact for applications to planetary atmospheres and astrophysics, in *Charged Particle and Photon Interactions With Matter: Recent Advances, Applications, and Interfaces*, edited by Y. Hatano, Y. Katsumura, and A. Mozumder, pp. 761–804, CRC Press, Boca Raton, Fla., doi:10.1201/b10389-29.

Ajello, J. M., R. A. West, C. P. Malone, J. Gustin, L. W. Esposito, W. E. McClintock, G. M. Holsclaw, and M. H. Stevens (2011a), Cassini UVIS observations of Titan ultraviolet airglow spectra with laboratory modeling from electron- and proton-excited N2 emission studies, Abstract SA11A-05, presented at 2011 Fall Meeting, AGU, San Francisco, Calif., 5–9 Dec.

Ajello, J. M., R. Mangina, D. Strickland, and D. Dziczek (2011b), Laboratory studies of UV emissions from proton-impact on N_2: The Lyman-Birge-Hopfield band system for aurora analysis, *J. Geophys. Res.*, 116, A00K03, doi:10.1029/2010JA016103.

Bishop, J., and P. D. Feldman (2003), Analysis of the Astro-1/Hopkins Ultraviolet Telescope EUV–FUV dayside nadir spectral radiance measurements, *J. Geophys. Res.*, 108(A6), 1243, doi:10.1029/2001JA000330.

Bishop, J., M. H. Stevens, and P. D. Feldman (2007), Molecular nitrogen Carroll-Yoshino v′ = 0 emission in the thermospheric dayglow as seen by the Far Ultraviolet Spectroscopic Explorer, *J. Geophys. Res.*, 112, A10312, doi:10.1029/2007JA012389.

Broadfoot, A. L., et al. (1997), N_2 triplet band systems and atomic oxygen in the dayglow, *J. Geophys. Res.*, 102, 11,567–11,584, doi:10.1029/97JA00771.

Cravens, T. E., I. P. Robertson, S. A. Ledvina, D. S. M. Mitchell, and S. M. Krimigis (2008), Energetic ion precipitation at Titan, *Geophys. Res. Lett.*, 35, L03103, doi:10.1029/2007GL032451.

Cravens, T. E., R. V. Yelle, J.-E. Wahlund, D. E. Shemansky, and A. F. Nagy (2009), Composition and structure of the Ionosphere and thermosphere, in *Titan From Cassini–Huygens*, edited by R. Brown, J.-P. Lebreton, and H. Waite, pp. 259–295, Springer, Dordrecht, Netherlands, doi:10.1007/978-1-4020-9215-2_11.

De La Haye, V., et al. (2007), Cassini Ion and Neutral Mass Spectrometer data in Titan's upper atmosphere and exosphere: Observation of a suprathermal corona, *J. Geophys. Res.*, 112, A07309, doi:10.1029/2006JA012222.

Esposito, L. W., et al. (2004), The Cassini Ultraviolet Imaging Spectrograph investigation, *Space Sci. Rev.*, 115, 299–361, doi:10.1007/s11214-004-1455-8.

Feldman, P. D., D. J. Sahnow, J. W. Kruk, E. M. Murphy, and H. Warren Moos (2001), High-resolution FUV spectroscopy of the terrestrial day airglow with the Far Ultraviolet Spectroscopic Explorer, *J. Geophys. Res.*, 106, 8119–8129, doi:10.1029/2000JA000356.

Fulchignoni, M., et al. (2005), In situ measurements of the physical characteristics of Titan's environment, *Nature*, 438, 785–791, doi:10.1038/nature04314.

Gan, L., C. N. Keller, and T. E. Cravens (1992), Electrons in the ionosphere of Titan, *J. Geophys. Res.*, 97, 12,137–12,151, doi:10.1029/92JA00300.

Gladstone, G. R., S. A. Stern, and W. R. Pryor (2012, in press), New Horizons cruise observations of Lyman-α emissions from the interplanetary medium, in *Cross-Calibration of Far UV Spectra of Solar System Objects and the Heliosphere*, ISSI Sci. Rep. Ser., vol. 13, edited by E. Quémerais, M. Snow, and R.-M. Bonnet, pp. 175–188, Int. Space Sci. Inst., Bern, Switzerland.

Kameta, K., et al. (2002), Photoabsorption, photoionization, and neutral-dissociation cross sections of simple hydrocarbons in the vacuum ultraviolet range, *J. Electron Spectrosc. Relat. Phenom.*, 123, 225–238, doi:10.1016/S0368-2048(02)00022-1.

Kliore, A. J., et al. (2008), First results from the Cassini radio occultations of the Titan ionosphere, *J. Geophys. Res.*, 113, A09317, doi:10.1029/2007JA012965.

Lavvas, P., M. Galand, R. V. Yelle, A. N. Heays, B. R. Lewis, G. R. Lewis, and A. J. Coates (2011), Energy deposition and primary chemical products in Titan's upper atmosphere, *Icarus*, 213(1), 233–251, doi:10.1016/j.icarus.2011.03.001.

Lean, J. T., T. N. Woods, F. G. Eparvier, R. R. Meier, D. J. Strickland, J. T. Correira, and J. S. Evans (2011), Solar extreme ultraviolet irradiance: Present, past and future, *J. Geophys. Res.*, 116, A01102, doi:10.1029/2010JA015901.

Ledvina, S. A., T. E. Cravens, and K. Keckemety (2005), Ion distribution in Saturn's magnetosphere near Titan, *J. Geophys. Res.*, 110, A06211, doi:10.1029/2004JA010771.

Lewis, B. R., et al. (2005a), Lifetime and predissociation yield of $^{14}N_2$ $b^1\Pi_u$(v = 1) revisited: Effects of rotation, *J. Chem. Phys.*, 123, 236101, doi:10.1063/1.2137722.

Lewis, B. R., et al. (2005b), Predissociation mechanism for the lowest $^1\Pi_u$ states of N_2, *J. Chem. Phys.*, 122, 144302, doi:10.1063/1.1869986.

Lewis, B. R., et al. (2008a), Optical observation of the C, $3s\sigma_g F_3$, and $3p\pi_u G_3$ $^3\Pi_u$ states of N_2, *J. Chem. Phys.*, 129, 164305, doi:10.1063/1.2990655.

Lewis, B. R., et al. (2008b), A coupled-channel model of the $^3\Pi_u$ states of N_2: Structure and interactions of the $3s\sigma_g F_3 ^3\Pi_u$ and $3p\pi_u G_3$ $^3\Pi_u$ Rydberg states, *J. Chem. Phys.*, 129, 164306, doi:10.1063/1.2990656.

Liu, X., D. E. Shemansky, M. Ciocca, I. Kanik, and J. M. Ajello (2005), Analysis of the physical properties of the N_2 $c'^1\Sigma_u^+(0)$-$X^1\Sigma_g^+(0)$ transition, *Astrophys. J*, 623, 579–584, doi:10.1086/428641.

Liu, X., D. E. Shemanksy, C. Malone, P. Johnson, J. M. Ajello, I. Kanik, A. Heays, B. Lewis, S. Gibson, and G. Stark (2008), Experimental and coupled channels investigation of the radiative properties of the N_2 c′ $^1\Sigma_u^+$- X Σ_g^+ band system, *J. Geophys. Res.*, 113, A02304, doi:10.1029/2007JA012787.

Mangina, R. S., J. M. Ajello, and G. K. James (2011), High-resolution electron-impact emission spectra and vibrational emission cross sections from 330–1100 nm for N_2, *Astrophys. J.*, 196(1), 13, doi:10.1088/0067-0049/196/1/13.

Meier, R. R., J. A. R. Samson, Y. Chung, E.-M. Lee and Z.-X. He (1991), Production of N^+* from $N_2 + h\nu$: Effective EUV emission yields from laboratory and dayglow data, *Planet. Space Sci.*, 39, 1197–1207, doi:10.1016/0032-0633(91)90171-6.

Melin, H., D. E. Shemansky, and X. Liu (2009), The distribution of atomic hydrogen and oxygen in the magnetosphere of Saturn, *Planet. Space Sci.*, 438(14–15), 1743–1753, doi:10.1016/j.pss.2009.04.014.

Morrison, M. D., C. W. Bowers, and P. D. Feldman (1990), The EUV dayglow at high spectral resolution, *J. Geophys. Res.*, 95, 4113–4127, doi:10.1029/JA095iA04p04113.

Mumma, M. J., and E. C. Zipf (1971), Dissociative excitation of vacuum-ultraviolet emission features by electron impact on molecular gases, 2, N_2, *J. Chem. Phys.*, 55, 5582–5588, doi:10.1063/1.1675725.

Roncin, J. Y., J. L. Subtil, and F. Launay (1998), The high-resolution vacuum ultraviolet emission spectrum of molecular nitrogen from 82.6 to 124.2 nm: Level energies of 10 excited singlet electronic states, *J. Mol. Spectrosc.*, 188, 128–137, doi:10.1006/jmsp.1997.7497.

Rymer, A. M., H. T. Smith, A. Weellbrock, A. J. Coaters, and D. T. Young (2009), Discrete classification and electron energy spectra of Titan's varied magnetospheric environment, *Geophys. Res. Lett.*, 36, L15109, doi:10.1029/2009GL039427.

Samson, J. A. R., Y. Chung, and E.-M. Lee (1991), Excited ionic and neutral fragments produced by dissociation of the N_2^* H band, *J. Chem. Phys.*, 95, 717–719, doi:10.1063/1.461424.

Shah, M. B., C. J. Latimer, E. C. Latimer, E. C. Montenegro, O. J. Tucker, R. E. Johnson, and H. T. Smith (2009), The implantation and interactions of O^+ in Titan's atmosphere: Laboratory measurements of collision-induced dissociation of N_2 and modeling of positive ion formation, *Astrophys. J.*, 703, 1947–1954, doi:10.1088/0004-637X/703/2/1947.

Shemansky, D. E. (1969), N_2 Vegard-Kaplan system in absorption, *J. Chem. Phys.*, 51, 689–700, doi:10.1063/1.1672058.

Shemansky, D. E., I. Kanik and J. M. Ajello (1995), Fine-structure branching in N_2 c_4' $^1\Sigma_u^+(0)$, *Astrophys. J.*, 452, 480–485, doi:10.1086/176320.

Shemansky, D., I. Stewart, R. West, L. Esposito, J. Hallett, and X. Liu (2005), The Cassini UVIS stellar probe of the Titan atmosphere, *Science*, 308, 978, doi:10.1126/science.1111790.

Sittler, E. C., R. E. Hartle, C. Bertucci, A. Coates, T. E. Cravens, I. Dandouras, and D. Shemansky (2010a), Energy deposition processes in Titan's upper atmosphere and its induced magnetosphere, in *Titan From Cassini–Huygens*, edited by R. Brown, J.-P. Lebreton, and H. Waite, pp. 393–454, Springer, Dordrecht, Netherlands.

Sittler, E. C., et al. (2010b), Saturn's magnetospheric interactions with Titan as defined by Cassini encounters T9 and T18: New results, *Planet. Space Sci.*, 58, 327–350, doi:10.1016/j.pss.2009.09.017.

Smith, H. T., D. G. Mitchell, R. E. Johnson, and C. P. Paranicas (2009), Investigation of energetic proton penetration in Titan's atmosphere using

the Cassini INCA instrument, *Planet. Space Sci.*, *57*, 1538–1546, doi:10.1016/j.pss.2009.03.013.

Stevens, M. H. (2001), The EUV airglow of Titan: Production and loss of N_2 $c'_4(0)–X$, *J. Geophys. Res.*, *106*, 3685–3689, doi:10.1029/1999JA000329.

Stevens, M. H., et al. (2011), The production of Titan's ultraviolet nitrogen airglow, *J. Geophys. Res.*, *116*, A05304, doi:10.1029/2010JA016284.

Strobel, D., and J. Cui (2012 in press), Titan's upper atmosphere/exosphere, escape processes, and rates, in *Titan: Interior, Surface, Atmosphere, and Space Environment*, *Cambridge Planet. Sci. Ser.*, vol. 14, edited by I. Müller-Wodarg et al., pp. 279–295, Cambridge Univ. Press, Cambridge, U. K.

Tomasko, M. G., and R. A. West (2010), Aerosols in Titan's atmosphere, in *Titan From Cassini–Huygens*, edited by R. Brown, J.-P. Lebreton, and H. Waite, pp. 297–321, Springer, Dordrecht, Netherlands, doi:10.1007/978-1-4020-9215-2_12.

Ubachs, W., et al. (2001), Lifetime measurements on the c'_4 $^1\sum_u^+$, $v = 0, 1$ and 2 states of molecular nitrogen, *Chem. Phys.*, *270*, 215–225, doi:10.1016/S0301-0104(01)00378-0.

Vinatier, S., et al. (2007), Vertical abundance profiles of hydrocarbons in Titan's atmosphere at 15°S and 80°N retrieved from Cassini/CIRS spectra, *Icarus*, *188*(1), 120–138, doi:10.1016/j.icarus.2006.10.031.

West, R. A., J. M. Ajello, M. H. Stevens, J. S. Evans, and R. S. Mangina (2011), Airglow emission from Titan during eclipse, paper presented at EPSC-DPS Joint Meeting 2011, Nantes, France, 2–7 Oct.

West, R. A., J. M. Ajello, M. H. Stevens, D. F. Strobel, G. R. Gladstone, J. S. Evans, and E. T. Bradley (2012), Titan airglow during eclipse, *Geophys. Res. Lett.*, *39*, L18204, doi:10.1029/2012GL053230.

Westlake, J. H., J. M. Bell, J. H. Waite, R. E. Johnson, J. G. Luhmann, K. E. Mandt, B. A. Magee, and A. M. Rymer (2011), Titan's thermospheric response to various plasma environments, *J. Geophys. Res.*, *116*, A03318, doi:10.1029/2010JA016251.

Wilson, E. H. W., and S. K. Atreya (2004), Current state of modeling the photochemistry of Titan's mutually dependent atmosphere and ionosphere, *J. Geophys. Res.*, *109*, E06002, doi:10.1029/2003JE002181.

Young, J. A., et al. (2010), Lyman-Birge-Hopfield emissions from electron-impact excited N_2, *J. Phys. B At. Mol. Opt. Phys.*, *43*, 135201, doi:10.1088/0953-4075/43/13/135201.